UCSF
UC San Francisco Previously Published Works

Title

A CD22-Shp1 phosphatase axis controls integrin β_7 display and B cell function in mucosal immunity.

Permalink

https://escholarship.org/uc/item/27j4g9rr

Journal

Nature immunology, 22(3)

ISSN

1529-2908

Authors

Ballet, Romain
Brennan, Martin
Brandl, Carolin
et al.

Publication Date

2021-03-01

DOI

10.1038/s41590-021-00862-z

Peer reviewed

eScholarship.org Powered by the California Digital Library
University of California

Europe PMC Funders Group
Author Manuscript
Nat Immunol. Author manuscript; available in PMC 2021 August 15.

Published in final edited form as:
Nat Immunol. 2021 March 01; 22(3): 381–390. doi:10.1038/s41590-021-00862-z.

A CD22-Shp1 phosphatase axis controls integrin β_7 display and B cell function in mucosal immunity

Romain Ballet[1,2,#], **Martin Brennan**[1,2,10], **Carolin Brandl**[3,10], **Ningguo Feng**[1,4], **Jeremy Berri**[1,2], **Julian Cheng**[1,2], **Borja Ocón**[1,2], **Amin Alborzian Deh Sheikh**[5], **Alex Marki**[6], **Yuhan Bi**[1,2], **Clare L. Abram**[7], **Clifford A. Lowell**[7], **Takeshi Tsubata**[5], **Harry B. Greenberg**[1,4], **Matthew S. Macauley**[8,9], **Klaus Ley**[6], **Lars Nitschke**[3], **Eugene C. Butcher**[1,2,#]

[1]The Center for Molecular Biology and Medicine, Veterans Affairs Palo Alto Health Care System and The Palo Alto Veterans Institute for Research, Palo Alto, CA, United States

[2]Laboratory of Immunology and Vascular Biology, Department of Pathology, School of Medicine, Stanford University, Stanford, CA, United States

[3]Division of Genetics, Department of Biology, University of Erlangen-Nürnberg, Erlangen, Germany

[4]Departments of Medicine and Microbiology and Immunology, School of Medicine, Stanford University, Stanford, California, USA

[5]Department of Immunology, Medical Research Institute, Tokyo Medical and Dental University, Tokyo, Japan

[6]La Jolla Institute for Allergy and Immunology, La Jolla, California, USA

[7]Department of Laboratory Medicine and the Program in Immunology, University of California, San Francisco, San Francisco

[8]Department of Chemistry, University of Alberta, Edmonton, Alberta, Canada

[9]Department of Medical Microbiology and Immunology, University of Alberta, Edmonton, Alberta, Canada

Abstract

Users may view, print, copy, and download text and data-mine the content in such documents, for the purposes of academic research, subject always to the full Conditions of use:http://www.nature.com/authors/editorial_policies/license.html#terms

[#]Corresponding authors: - ballet.r@gmail.com - ebutcher@stanford.edu.
[10]These authors contributed equally to the work.

Author contributions

R.B. conceptualized the study, designed, performed, analyzed the majority of the experiments, and wrote the manuscript. M.B. performed and analyzed PLA experiments and all confocal microscopy experiments; C.B. performed experiments involving the *Cd22*^{Y256F} and *Cd22*^{R130E} transgenic animals; N.F. performed oral RV infections, and helped conceptualizing and designing the RV studies; J.B. and J.C. contributed to the analysis of the video microcopy experiments; B.O. performed gut preparations in the RV studies and helped with SI fragment cultures; A.M. shared his intravital microscopy expertise with R.B.; Y.B. helped in RT-PCR studies; A.A.D.S. and T.T. helped conceptualizing PLA studies; C.A.L and C.L.A. provided the *motheathen viable* mice; H.B.G. contributed to conceptualizing and designing the RV studies; M.S.M., K.L. and L.N. contributed to conceptualizing the study and provided intellectual input; E.C.B. guided, conceptualized and supervised the study, and wrote the manuscript.

Competing interests

The authors declare no competing interests.

Europe PMC Funders Author Manuscripts
Europe PMC Funders Author Manuscripts

Europe PMC Funders Author Manuscripts

Europe PMC Funders Author Manuscripts

The integrin $\alpha_4\beta_7$ selectively regulates lymphocyte trafficking and adhesion in the gut and gut-associated lymphoid tissues (GALT). Here we describe unexpected involvement of tyrosine phosphatase Shp1 and the B cell lectin CD22 (Siglec 2) in regulation of $\alpha_4\beta_7$ surface expression and gut immunity. Shp1 selectively inhibited β_7 endocytosis, enhancing surface $\alpha_4\beta_7$ display and lymphocyte homing to GALT. In B cells, CD22 associated in a sialic acid-dependent manner with integrin β_7 on the cell surface to target intracellular Shp1 to β_7. Shp1 restrained plasma membrane β_7 phosphorylation and inhibited β_7 endocytosis without affecting β_1 integrin. B cells with reduced Shp1 activity, B cells lacking CD22, or B cells expressing CD22 with mutated Shp1-binding or carbohydrate-binding domains displayed parallel reductions in surface $\alpha_4\beta_7$ and in homing to GALT. Consistent with the specialized role of $\alpha_4\beta_7$ in intestinal immunity, CD22 deficiency selectively inhibited intestinal antibody and pathogen responses.

Introduction

The integrin $\alpha_4\beta_7$ functions as a B and T cell adhesion receptor for the mucosal vascular addressin (MAdCAM-1) expressed by postcapillary high endothelial venules (HEVs) in GALT, and by, lamina propria venule sites of effector cell recruitment, and by stromal cells in GALT[1–3]. GALT are the major sites of B cell activation and humoral immune induction for intestinal immunity. Activated B cells undergo isotype class switching in Peyer's patches (PPs) and differentiate into migratory immunoglobulin A (IgA)-secreting plasmablasts that use $\alpha_4\beta_7$ to home to mucosal surfaces[4] where local production of secretory IgA provides immune protection. Presumably in support of this role, B cells home preferentially to and predominate in murine PPs, contrasting with peripheral lymph nodes (PLNs) where T cells are the majority[5]. This homing preference correlates with higher surface expression of $\alpha_4\beta_7$ on B cells than on T cells[6], but the mechanisms responsible for this differential $\alpha_4\beta_7$ surface expression and its essential role in intestinal immunity have not been defined.

The tyrosine phosphatase Shp1 (Src homology region 2 domain-containing phosphatase-1, encoded by the gene *Ptpn6*) has essential roles in regulating immune homeostasis: homozygous gene depletion of *Ptpn6* as described in the *motheathen* mice (*Ptpn6* $^{me/me}$) results in severe systemic inflammation and death within weeks[7]. The closely related *motheathen viable* mutant mice (*Ptpn6* $^{meV/meV}$) express wild-type levels of Shp1 but the catalytic activity of the enzyme is greatly reduced, resulting in a similar yet slightly less severe phenotype[8]. Shp1 plays essential roles in the regulation of tyrosine phosphorylation in T and B cells[9,10]. Shp1 can be targeted by its binding to phosphorylated ITIM (Immunoreceptor tyrosine-based inhibitory motif) sequences in membrane receptors, often acting in conjunction with ITIM-bearing molecules to inhibit signaling pathways including those involved in integrin activity. In T cells for example, Shp1 controls the deactivation of the LFA-1 integrin ($\alpha_L\beta_2$) to prevent aberrant adhesion of leukocytes to β_2 integrin ligands or T cell adhesion to antigen presenting cells[11]. In B cells, upon antigen stimulation, the phosphorylated ITIM sequences of CD22 (Sialic acid-binding Ig-like lectin 2 or Siglec-2) recruit Shp1 to inhibit downstream components of the B cell antigen receptor (BCR)-induced Ca^{2+} signaling[12]. However, Shp1 has not been implicated in control of integrin endocytosis or cell surface expression.

Europe PMC Funders Author Manuscripts

Europe PMC Funders Author Manuscripts

Here, we report that the pair Shp1/Cd22 acts in a cell-intrinsic manner to enhance $\alpha_4\beta_7$ surface abundance, with profound organotypic effects on mucosal immune responses. The findings uncover a selective role for Shp1 in $\alpha_4\beta_7$ endocytosis and surface expression, define CD22 ITIM- and lectin/carbohydrate-dependent mechanisms targeting Shp1 to β_7 integrin in B cells, and support the significance of these mechanisms to efficient intestinal antibody (Ab) responses.

Results

Shp1 augments $\alpha_4\beta_7$ cell surface display in lymphocytes

In studies of *motheaten viable* mutant mice (*Ptpn6* $^{meV/meV}$) lacking Shp1 activity, immunofluorescent staining with antibodies to the $\alpha_4\beta_7$ heterodimer or to the β_7 subunit revealed a substantial (~ 90%) reduction in the median fluorescence intensity (MFI) of *Ptpn6* $^{meV/meV}$ splenic naïve B cells as compared to wild-type controls. The α_4 subunit, which forms heterodimers with integrin β_1 as well as β_7, was reduced ~ 20% in *Ptpn6* $^{meV/meV}$ B cells reflecting the reduction in $\alpha_4\beta_7$. In contrast, we found no reduction for integrins α_L, β_1, and β_2 (Fig. 1a). β_7 was also reduced on $CD4^+$ and $CD8^+$ T cells (Fig. 1a). Since the *Ptpn6* $^{meV/meV}$ phenotype induces profound changes in the phenotype and homeostasis of mature B cells[13] and T cells[14,15], we repeated the above experiments with heterozygous *motheaten viable* mice (*Ptpn6* $^{+/meV}$). α_4, β_7, and $\alpha_4\beta_7$ integrins were also reduced on heterozygous *Ptpn6* $^{+/meV}$ B and T cells, while α_L, β_1, and β_2 were not affected (Fig. 1b). Thus Shp1 positively regulates the cell surface abundance of integrin $\alpha_4\beta_7$ on lymphocytes without affecting other integrins.

CD22 mediates the Shp1-dependent $\alpha_4\beta_7$ effects in B cells

The selective effect of the *Ptpn6* $^{+/meV}$ phenotype on B cells suggested potential involvement of CD22, a B cell specific lectin known to recruit Shp1 to the plasma membrane through interactions with its cytoplasmic ITIM sequences[12]. B cells from *Cd22* $^{-/-}$ mice showed reduced surface α_4, β_7, and $\alpha_4\beta_7$ expression by flow cytometry and confocal microscopy, but normal expression of α_L and β_1 (Fig. 2b,c,e). B cells isolated from the blood, the bone marrow (BM), PLNs and PPs of *Cd22* $^{-/-}$ animals displayed a similar reduction in $\alpha_4\beta_7$ (Fig. 2f). Consistent with selective expression of CD22 by B cells, CD22 deficiency had no effect on $CD4^+$ T cell integrins (Extended Data Fig. 1). mRNA expression of the β_7 subunit in wild-type and *Cd22* $^{-/-}$ B cells was unchanged (Fig. 2g) and subcellular imaging showed similar levels of intracellular β_7 in wild-type and mutant cells, far above cell surface levels (Fig. 2d,e), ruling out an effect of CD22 deficiency on *Itgb7* gene expression and protein synthesis. Intracellular Shp1 spots co-localized with cell surface β_7 in wild-type B cells more often than in *Cd22* $^{-/-}$ B cells (Fig 2h,i). In wild-type cells, most of these β_7–Shp1 interactions aligned with clusters of CD22 (>80%, Fig. 2h,j).

These data suggest that CD22 mediates the Shp1 augmentation of cell surface $\alpha_4\beta_7$. If so, we reasoned that mutation of the Shp1-binding cytoplasmic ITIM motifs in CD22 should mimic CD22 deficiency. To address this, we used transgenic animals ($CD22^{Y2,5,6F}$) in which the CD22 ITIM signaling domains has been mutated[16] to prevent Shp1 binding and downstream CD22 signaling (Fig. 2a). B cells in $CD22^{Y2,5,6F}$ express normal amounts of

Europe PMC Funders Author Manuscripts

Europe PMC Funders Author Manuscripts

CD22[16]. CD22^{Y2,5,6F} B cells displayed surface abundance of α_4, β_7, and $\alpha_4\beta_7$ as severely reduced as on *Cd22* $^{-/-}$ B cells, again with no effect on the other integrin surface expression (Fig. 2b).

CD22 is a lectin that interacts in *cis* with α2-6 sialic acid(α2-6 Sia)-decorated glycoproteins such as CD22[17] or CD45[18], affecting its distribution and motility on the B cell surface[19]. To assess a potential role for the CD22 lectin-carbohydrate interactions in cell autonomous $\alpha_4\beta_7$ regulation, we assessed integrin cell surface levels by B cells expressing a mutated lectin domain (CD22^{R130E}) that prevents α2-6 Sia binding[16] (Fig. 2a). CD22^{R130E} B cells expressed CD22 at wild-type levels[16], and displayed a significant reduction in $\alpha_4\beta_7$ levels (Fig. 2b), although the effect was less severe than that of CD22 deficiency or ITIM mutations. Intermediate reduction in $\alpha_4\beta_7$ was also observed in B cells from *St6Gal1* $^{-/-}$ mice, which lack α2-6 sialyltransferase activity[20] and thus CD22 ligands (Extended Data Fig. 2).

α2-6 Sia-dependent CD22-β_7 association at the cell surface

The reduction of β_7 in the absence of CD22 lectin activity suggests cell surface interactions between CD22 and β_7. Using proximity ligation assay (PLA) in resting B cells, we detected a robust PLA signal between CD22 and β_7 (~5-6 spots per cell) (Fig. 3a), but there was no interaction of CD22 and β_1 (Fig. 3b). A strong CD22-independent PLA signal was observed with anti-β_1 and anti-α_4 antibodies (detecting $\alpha_4\beta_1$ heterodimer interactions), confirming the activity and specificity of the β_1 antibody (Fig. 3c). To assess dependence on sialic acid, we pre-treated purified B cells with *Arthrobacter ureafaciens* sialidase at a concentration that retained cell viability while reducing Sambucus Nigra Lectin (SNA) (α2-6 Sia binding lectin) staining by ~60% (Extended Data Fig. 3). Sialidase-treated wild-type B cells showed significantly reduced association between CD22 and β_7 compared to untreated wild-type cells (Fig. 3a). Together, the data show cell surface sialic acid-dependent CD22 association with integrin β_7 but not β_1.

Shp1-CD22 inhibits β_7 endocytosis in B cells

Cell surface receptor expression is regulated by endocytosis and recycling[21]. We compared the effects of CD22 or Shp1 deficiency on endocytosis of β_7 vs. β_1 integrins and of the transferrin receptor as a control that undergoes endocytic recycling. We assessed internalization by flow cytometry using pHrodo-Red, a dye whose fluorescence increases within the acidic pH of endocytic vesicles. We incubated splenocytes at 37°C to enable endocytosis in the presence of pHrodo-red-conjugated transferrin (Tf), anti-β_7, anti-β_1, or isotype matched control Abs. Background was defined by staining of cells with the pHrodo-Red constructs incubated at 4°C to prevent endocytosis. Endocytosis, defined by the internalization-induced (background corrected) pHrodo-Red signal, was normalized to cell surface expression of each antigen at 4°C to yield a Relative Endocytosis Ratio (RER, Fig. 4a).

CD22-deficient B cells displayed a significantly higher RER for integrin β_7 compared to wild-type B cells (1.65 fold higher, $p<0.0001$). CD22-deficiency did not alter the basal endocytosis of Tf, or of integrin β_1 (Fig. 4b), and endocytosis was not observed for the

Europe PMC Funders Author Manuscripts

Europe PMC Funders Author Manuscripts

isotype control Abs (not shown). *Ptpn6* $^{+/meV}$ B cells showed a shift similar to that of CD22^{-}/– cells, but not reaching significance. Treatment of cells with primaquine (PQ) to inhibit recycling of proteins back to the plasma membrane[22] increased internalization and the differences between *Ptpn6* $^{+/meV}$ and wild-type B cells (RER 1.54 vs. 1.18, $p<0.05$) and *St6Gal1* $^{-/-}$ vs. wild-type cells (1.59 vs. 1.18, $p<0.01$); and PQ treatment enhanced the difference between *Cd22* $^{-/-}$ and wild-type B cells (2.84 vs. 1.18, $p<0.0001$) (Fig. 4b). The results suggest that loss of CD22 or reduction of Shp1 activity (*Ptpn6* $^{+/meV}$) similarly and selectively inhibit β_7 endocytosis in B cells.

Shp1-CD22 restrains plasma membrane β_7 phosphorylation

Integrin beta tails, including that of β_7, comprise conserved motifs for tyrosine phosphorylation by Src family kinases, regulating integrin functions[23–25]. These motifs interact with a large number of phosphotyrosine binding (PTB) domain-containing proteins, including proteins that regulate endocytic trafficking[25–28]. To determine if CD22 restrains the phosphorylation of β_7 at the cell surface, we compared tyrosine phosphorylation of cell surface vs. intracellular β_7 in CD22-deficient vs. wild-type B cells. We biotinylated cell surface proteins by incubation of cells with sulfo-NHS-biotin at 4°C to prevent protein internalization (Fig. 5a). We isolated cell surface β_7 from purified B or T cell lysate using successive immunoprecipitations (IP) for β_7 with the β_7-specific antibody FIB504 and then for biotin with streptavidin-conjugated beads (SA-IP). We recovered cell surface β_7 from the eluate of the SA-IP and intracellular β_7 from the biotin-free flow through prior to quantification of β_7 and phosphotyrosine (p-Tyr) by immunoblot (Fig. 5a). We found a significant increase of p-Tyr (normalized to β_7) in the cell surface β_7 fraction of *Ptpn6* $^{+/meV}$ and *Cd22* $^{-/-}$ B cells compared to wild-type controls (Fig. 5b), whereas phosphorylation of intracellular β_7 did not differ in mutants vs. wild-type (Fig. 5b). The p-Tyr/β_7 ratio among the cell surface β_7 fraction of *Ptpn6* $^{+/}$ meV and *Cd22* $^{-/-}$ B cells reached levels similar to the intracellular pool. In contrast to the effects of CD22 deficiency on surface β_7 phosphorylation in B cells, we found no difference in cell surface p-Tyr/β_7 ratios in *Cd22* $^{-/-}$ T cells compared to wild-type T cells (Extended Data Fig. 4). In conjunction with the known role of phosphorylation in endocytosis, the results suggest that tyrosine phosphorylation of β_7 at the cell surface functions as a switch to enhance β_7 endocytosis and that the CD22/Shp1 axis shifts the balance of p-Tyr towards β_7 dephosphorylation to maintain the integrin at the cell surface.

Shp1-CD22 enhances B cell homing to GALT

To assess the consequence of Shp1/CD22-dependent $\alpha_4\beta_7$ regulation in GALT, we first assessed lymphocyte composition of *Cd22* $^{-/-}$ and wild-type PPs. PPs from mutant and wild-type animals were similar in number and size, but mutant PP had a significant decrease (~70%) in naive B cell numbers compared to wild-type PPs (Fig. 6a). There was no difference in germinal center or activated B cells (GC/A, CD19^{+} IgD^{-}) or T cell numbers (Fig. 6b and Extended Data Fig. 5). We found no difference in the PLNs, taken as controls, showing the specificity of the effects for GALT (Fig. 6b).

We next assessed the short-term homing of mutant B cells into PPs and mesenteric lymph nodes (MLNs) which express the dedicated $\alpha_4\beta_7$ ligand MAdCAM-1. Recipient wild-type

Europe PMC Funders Author Manuscripts

Europe PMC Funders Author Manuscripts

mice received splenocytes from wild-type and mutant donors labeled with different cell tracker dyes and mixed at a 1:1:1 ratio as confirmed by flow cytometry. Two hours later, we enumerated cells localized to PPs and MLNs by flow cytometry (Fig. 6c). In agreement with the reduction of $\alpha_4\beta_7$, *Ptpn6* $^{+/meV}$ B cells, *Cd22* $^{-/-}$ B cells, CD22^{Y2,5,6F} ITIM mutant B cells, and CD22^{R130E} lectin mutant B cells homed poorly to PPs, displaying a similar ~60% reduction in recruitment compared to wild-type B cells (Fig. 6d,e). We observed an intermediate defect for all mutant B cells in homing to the MLN that is consistent with MAdCAM-1 expression on subsets of MLN HEV, while homing to the PLNs, spleen and bone marrow, which is independent of $\alpha_4\beta_7$, was normal (Fig. 6d,e, and Extended Data Fig. 6). CD22 deficiency did not affect CD4$^+$ T cell homing to PPs while reduced Shp1 activity (*Ptpn6* $^{+/meV}$) compromised CD4$^+$ T cell homing consistent with reduced cell surface β_7 expression. *Ptpn6* $^{+/meV}$ CD4$^+$ T cells also localized poorly to PLNs (Extended Data Fig. 7): this may reflect the role of Shp1 in modulating β_2 integrin activity in T cells[11].

$\alpha_4\beta_7$ mediates activation-independent tethering and rolling on PP, and chemokine/integrin activation-dependent arrest in combination with LFA-1[2]. To assess the effects of the CD22/Shp1 axis on these steps, we visualized B and T cell behavior in PPs by intravital microscopy. We purified B or T cells from wild-type, *Ptpn6* $^{+/meV}$ and *Cd22* $^{-/-}$ donors, labeled them with different cell tracker dyes, mixed mutant and wild-type cells at a 1:1 ratio as confirmed by flow cytometry, and transferred the cells into a recipient wild-type mouse while imaging the PPs (Fig. 6f). We captured high frame rate movies (40 frames per second) to study the behavior of all cells entering HEV within the field of view during the recording (i.e. ~30-40 s). We stratified the cells into four groups based on their interactions with HEV: freely flowing cells that failed to interact detectably, termed flyers, appeared as streaks due to their high velocity during the time of exposure, and passed through the HEVs at a mean velocity of ~ 1000 μm/s (Extended Data Fig. 8a–c and Supplementary Video 1). Cell capture on the vessel wall could be visualized as soon as the cell looked round and bright as a result of reduced velocity. Cells attaching briefly (< 1s) before detaching and flying through the HEV were described as brief rollers (Extended Data Fig. 8b,c and Supplementary Video 2). Cells interacting for more than 1 sec were called rollers (Extended data Fig. 8b,c and Supplementary Video 3). Among rollers, cells static for more than 2 s at the end of the recording were considered “arresters”.

At the end of ~30 seconds of observation, the number of *Ptpn6* $^{+/meV}$ and *Cd22* $^{-/-}$ arrested B cells was ~50% and ~60% lower ($p<0.0001$) respectively than wild-type B cells (Fig. 6g,j; Supplementary Video 4,5). The reduced frequency of arrest correlated with inefficient initial capture or tethering, as well as faster rolling (looser interaction) of *Ptpn6* $^{+/meV}$ and *Cd22* $^{-/-}$ B cells. We observed a reduced frequency of rolling by *Ptpn6* $^{+/meV}$ and *Cd22* $^{-/-}$ B cells as compared to wild-type control cells with a corresponding increase in non-interacting flyers (Fig. 6h,k). Among rollers, the average rolling velocity of *Ptpn6* $^{+/meV}$ and *Cd22* $^{-/-}$ B cells was ~2-3 times higher than wild-type control (Fig. 6i,l; Supplementary Video 6,7). The total number of mutant cells and wild-type B cells entering PP-HEVs (including rollers, brief rollers, or flyers) was similar in each experiment, thus ruling out distortion of results by differences in retention of mutant cells in other organs (Extended Data Fig. 8d). The CD22 effect could be due to lack of interaction with HEV-expressed CD22 ligand: however, the parallel alterations in *Ptpn6* $^{+/meV}$ B cell behavior suggest that the cell intrinsic reduction of

Europe PMC Funders Author Manuscripts

Europe PMC Funders Author Manuscripts

$\alpha_4\beta_7$, which *Ptpn6* $^{+/meV}$ and CD22 deficient B cells have in common, is likely the major factor involved in reduced interaction efficiency and PP homing. Consistent with this hypothesis, the effects of CD22 deficiency and reduced Shp1 activity (*Ptpn6* $^{+/meV}$) on tethering and on rolling velocity were phenocopied by experimental reduction in surface $\alpha_4\beta_7$ available for interaction (Extended Data Fig. 9). Moreover, reduced $\alpha_4\beta_7$ on *Cd22* $^{-/-}$ B cells significantly impacts homing to the PP even in absence of the CD22-ligand on PP-HEVs (Extended Data Fig. 10).

We conclude that Shp1-driven CD22 regulation of β_7 drives enhanced B cell homing to GALT, and substantially augments the adhesive functions of the mucosal lymphocyte integrin $\alpha_4\beta_7$.

CD22 deficiency inhibits intestinal antibody responses

In addition to its roles in gut lymphocyte homing, $\alpha_4\beta_7$ mediates cell-cell interactions of lymphocytes with MAdCAM-1 expressed by follicular dendritic cells (FDCs) in GALT[29]. It also supports interactions of $\alpha_4\beta_7$-expressing lymphocytes with other ligands including α_4 on adjacent immune cells, fibronectin in the extracellular matrix, and VCAM-1[1,30]. Moreover, $\alpha_4\beta_7$ is highly expressed by B cells involved in gut immune responses, but is downregulated on B cells responding to systemic (non-intestinal) antigens[31–33]. Thus we reasoned that CD22-dependent $\alpha_4\beta_7$ surface expression might have a selective role in intestinal (vs. systemic) antibody responses. On the other hand, CD22 suppresses BCR responses in general, and its deficiency has been considered to enhance B cell activation.

To distinguish between these possibilities, we immunized wild-type and CD22-deficient mice with Cholera Toxin B (CTB) by different routes and compared the humoral responses two weeks later. CD22 deficiency caused a clear reduction in antigen specific IgA and IgG responses to oral CTB, but not to nasal or intramuscular immunization (Fig. 7a,c). Total IgA and IgG concentrations in the serum after oral, nasal, and intramuscular immunizations were similar in CD22 deficient vs. wild-type animals, ruling out a global inhibition or activation of B cell responses (Fig. 7b,d).

We also analyzed CTB-specific IgA and IgG production from *ex-vivo* cultures of small intestine (SI) segments. Intestinal CTB-specific IgA (Fig. 7e) and IgG (Fig. 7f) were decreased in *Cd22* $^{-/-}$ mice after oral immunization, and CTB-specific IgA after intramuscular immunization: but there was no significant alteration in SI IgA or IgG after intranasal immunization (Fig. 7e,f). The results suggest that the CD22-driven augmentation of $\alpha_4\beta_7$ surface expression selectively amplify gut-specific, but not systemic, antibody responses.

CD22 improves the antibody response to rotavirus

Rotavirus (RV) selectively infects intestinal epithelial cells, leading to strong immune responses in GALT; and the local production of RV-specific IgA plays a significant role in protection[34]. Young pups, more susceptible to infection than adults, were infected with RV. We measured total and RV-specific IgA and IgG in the feces daily. Ten days post infection (p.i.), wild-type animals started to mount robust RV-specific intestinal IgA and IgG responses (Fig. 8a,b), which preceded a reduction of fecal viral shedding by day 12 p.i. and a

Europe PMC Funders Author Manuscripts

Europe PMC Funders Author Manuscripts

full resolution of RV infection by day 15 p.i. (Fig. 8c). In contrast, CD22-deficient animals had a dramatically reduced RV-specific IgA response in the feces (Fig. 8a), and a delay in the resolution as indicated by residual viral shedding at day 12 p.i. (Fig. 8c). Virus was eliminated by day 15 p.i. in both wild-type and *Cd22*$^{-/-}$ mice (Fig. 8c).

At the peak of the fecal antibody response (day 12 p.i.) we observed reduced RV-specific IgA titers in the serum of CD22-deficient animals (Fig. 8d) while RV-specific IgG, total IgG and total IgA were similar to wild-type (Fig. 8d,e). *Cd22*$^{-/-}$ animals also had fewer RV-specific IgA antibody secreting B cells in MLNs and the small intestine lamina propria (SI LP) than wild-type mice at day 12 p.i., while there were no differences in the spleen (Fig. 8f). To determine whether the reduction of RV-specific fecal antibody in *Cd22*$^{-/-}$ mice reflected a deficit in local production in the gut (as opposed to altered antibody secretion in bile), we analyzed RV-specific IgA and IgG levels in *ex vivo* culture of SI segments. We found a two-fold decrease in the RV-specific IgA and IgG titers in CD22-deficient animals as compared to wild-type controls (Fig. 8g and 8h), which correlates with higher viral shedding in the feces at day 12 p.i. as mentioned above (Fig. 8c). Together, these data highlight a significant role of B cell CD22 in the mucosal pathogen response.

Discussion

We report a previously unappreciated contribution for the Shp1/CD22 complex in the cell autonomous regulation of the gut integrin receptor $\alpha_4\beta_7$. We show that Shp1 inhibits $\alpha_4\beta_7$ endocytosis and maintains cell surface $\alpha_4\beta_7$ expression. We show that B cell-specific Shp1-binding lectin CD22 associates with β_7 on the cell surface, specifically targeting Shp1 to β_7 and reducing β_7 tyrosine phosphorylation. Our results support a model in which this cascade inhibits $\alpha_4\beta_7$ endocytosis and degradation, resulting in higher surface expression of the gut homing integrin. We present evidence that this novel mechanistic cascade is functionally important not only in B cell homing to GALT but also in intestinal antibody responses. The results define a novel pathway for differential control of integrin function and an unexpected and selective role for a CD22-Shp1 axis in intestinal immunity.

Beta integrin phosphorylation controls integrin functions including activation[23,25,35] and endocytosis[28,36,37] by means of phosphotyrosine binding domain (PTB)-containing proteins that interact with integrin β tails such as Talin[38], Kindlin[38], Dok-1[23–25] or Phox-homology 4.1/ezrin/radixin/moesin (PX-FERM) domain-containing sortin nexins[39,40]. Our results suggest that Shp1 acts as a phosphorylation switch that directly or indirectly restrains tyrosine phosphorylation of integrin β_7, thus reducing β_7 endocytosis. On B cells, CD22 targeting of Shp1 to β_7 may also alter the phosphorylation state of other PTB-domain or FERM domain-containing targets in the vicinity of the integrin, potentially affecting endocytic adaptors[37] to inhibit endocytosis as well.

Beta7 (β_7) cell surface levels in *Cd22*$^{-/-}$ B cells are comparable to those on wild type naive T cells, suggesting that CD22 itself is enough to explain the higher surface expression of $\alpha_4\beta_7$ by normal naïve B versus T cells[6]. It is intriguing to speculate that alternative ITIM-containing proteins may regulate T cell β_7, perhaps contributing to the enhanced β_7 display by intestinal memory T cells.

Europe PMC Funders Author Manuscripts

Europe PMC Funders Author Manuscripts

On B cells, CD22 can associate in *cis* with α2-6 Sia modified membrane glycoproteins including CD22 itself and CD45: these *cis*-interactions can bring ITIM-bound Shp1 phosphatase in close proximity to target substrates, altering the phosphorylation state and function of associated molecules[12]. Using proximity ligation assays, we showed that β_7 but not β_1 integrin associates closely with CD22, a specific interaction that is dependent on cell surface sialic acid and that likely contributes to the magnitude and specificity of the effects. Yet the reduction of β_7 in lectin ($CD22^{R130E}$) and St6gal1-deficient mutants was less than that in ITIM ($CD22^{Y256F}$) mutants. In $CD22^{R130E}$ mutant B cells, CD22 itself is known to be more phosphorylated, recruits more Shp1, and has higher lateral mobility than in wild-type B cells[16,19]. These effects would be expected to allow CD22/Shp1 to access β_7 even in the absence of specific targeting, explaining the partial retention of surface levels in the absence of lectin activity ($CD22^{R130E}$) or CD22 ligand (*St6gal1* $^{-/-}$), and the intermediate effect on endocytosis seen with *St6Gal1* $^{-/-}$ B cells. Taken together, the data suggest that CD22–α2-6 Sia interactions recruit CD22-ITIM-docked Shp1 phosphatase to β_7 to alter the local tyrosine phosphorylation balance, inhibit β_7 endocytosis and enhance $\alpha_4\beta_7$ surface expression.

B cell positioning, activation and cell-cell interactions in the GALT, which all involve contributions from $\alpha_4\beta_7$, drive production of local and systemic antibodies to intestinal antigens and pathogens. Although CD22 deficient mice show grossly normal systemic B cell development[41], we observed a profound defect in the intestinal and systemic antigen (Ag)-specific IgA and IgG levels to oral immunization with Cholera-Toxin B in CD22-deficient animals, whereas the IgG response to nasal or intramuscular immunization was preserved. The results closely recapitulate the reported effects of β_7-deficiency or $\alpha_4\beta_7$ blockade which also selectively impair Ab responses to oral vs. systemic Ag[42]. Taking into account that CD22 is known to restrain B cell responses and that its deficiency may enhance them *in vivo* [43], the selective reduction of mucosal immune responses in CD22-deficient animals highlights the critical and dominant importance of the CD22-dependent β_7 regulation for optimal mucosal immunity. Accordingly, we found that CD22 deficiency impaired the response of mice to infection with rotavirus, a reovirus that selectively infects small intestinal epithelial cells and is a major cause of childhood diarrheal illness[44]. CD22 deficiency caused a significant reduction in viral clearance, comparable to that reported in mice with a complete lack of B cells[45], or lacking IgA[46], or lacking GALT[47] itself. The protective effect of CD22 deficiency likely reflects global influences of CD22-dependent $\alpha_4\beta_7$ functions in the intestinal immune response.

We previously showed that PP and MLN HEVs, but not PLN HEVs, express functional carbohydrate ligands for CD22, ligand encoded by *St6Gal1*. *St6Gal1* $^{-/-}$ PP-HEV are defective at recruiting CD22-expressing B cells in short-term homing assays[48], likely as a result of trans-interactions between CD22 and α2-6 Sia decorated glycans on HEVs. Yet we showed here that even in the absence of HEV CD22-ligands, the reduced $\alpha_4\beta_7$ on *Cd22* $^{-/-}$ B cells inhibits homing to the PP. In contrast to the effects of a defective CD22/Shp1 axis which inhibits tethering and speeds up rolling, intravital microscopy in *St6Gal1* $^{-/-}$-deficient mice revealed that wild-type B cells tether and roll normally on *St6Gal1* $^{-/-}$ PP-HEV: only definitive arrest is compromised (unpublished observations). We hypothesize that CD22 ligation to α2-6 Sia-modified MAdCAM-1 creates a synapse between CD22, MAdCAM-1

Europe PMC Funders Author Manuscripts

Europe PMC Funders Author Manuscripts

and $\alpha_4\beta_7$ facilitating chemokine-driven activation of $\alpha_4\beta_7$ and arrest of the B cell. An analogous mechanism controls the arrest of neutrophils: heterophilic ligation of endothelial cell expressed-CD99 to paired immunoglobulin-like receptors (PILRs) enhances the chemokine-induced β_2-dependent arrest of neutrophils on ICAM-1[49]. Future studies will likely shed light on this complex mechanism. It is fascinating that CD22 has evolved these two separate functions, (i) selective regulation of surface β_7 expression and (ii) trans-ligation to PP-HEVs heterophilic ligands, to serve the same goal of enhancing B cell homing to the GALT.

Methods

Reagents

All the antibodies used in these studies are listed in Supplementary Table 1 and in the Nature Research Reporting Summary linked to this article.

Mice

C57BL/6 wild-type mice, BALB/c wild-type mice, *Cd22*$^{-/-}$ mice[41], and *St6gal1*$^{-/-}$ mice[20] were bred and housed in the animal facilities of the Veterans Affairs Palo Alto Health Care System, accredited by the Association for Assessment and Accreditation of Laboratory Animal Care. CD22^{Y2,5,6F} mice[16] and CD22^{R130E} mice[16] were bred and housed at the Department of Biology of the University of Erlangen; *Ptpn6*$^{meV/meV}$ and *Ptpn6*$^{+/meV}$ mice[8] were bred and housed at the University of California San Francisco. All animals were housed under standard conditions, maintained in a 12 h/12 h light/dark cycle at 22°C ± 2 °C and were given food and tap water ad libitum. Unless otherwise stated, 6–12-week-old male and female mice were used in all experiments. All animal work and housing conditions were approved by the Institutional Animal Care and Use Committee at the Veterans Affairs Palo Alto Health Care System, or by relevant animal care committees at the University of Erlangen.

Integrin expression and lymphocyte cellularity by flow cytometry

Lymphocytes from the blood, PLNs (inguinal, axillary and brachial lymph nodes), MLNs, BM, and PPs (average of 5 PPs per mouse) of wild-type and mutant mice were isolated and stained with fluorescently labeled antibodies against CD4, CD3ε, CD19, IgD and either α_L, β_2, α_4, β_1, β_7, $\alpha_4\beta_7$, or the appropriate Isotype Control. The Fc receptors were blocked using Rat Serum and anti-CD16/32 prior to the staining. Dead cells were excluded by staining with 4',6-diamidino-2-phénylindole (DAPI) or the LIVE/DEAD Fixable Aqua dye (Invitrogen). For integrin expression studies, the median fluorescence intensity (MFI) of isotype control was substracted to the MFI of the integrin staining. The integrin staining MFI (background corrected) was expressed as a percentage of the wild-type C57BL/6 (control group) mean MFI. For the cellularity studies, we added CountBright counting beads (Invitrogen) to each sample to calculate absolute cell number per organ. Samples were acquired on a Fortessa flow cytometer (BD Biosciences) using FACSDiva Software (BD, version 8.0.1) and were analyzed using FlowJo (BD, 10.3). A representative gating strategy is shown in Supplementary Fig. 1.

Europe PMC Funders Author Manuscripts

Europe PMC Funders Author Manuscripts

In-situ video microscopy analyses of lymphocyte interactions with PP-HEV

Naïve B cells or $CD4^+$ T cells were isolated from wild-type and *Cd22*$^{-/-}$ or *Ptpn6*$^{+/meV}$ splenocytes using negative selection kits (STEMCELL Technologies). For each experiment, the quality of the isolation was checked by flow cytometry and consisted of ≥98% cells of interest. Lymphocytes were labeled with 2.5 μM CMFDA (Invitrogen) or CMTPX (Invitrogen) for 10 min at 37°C in RPMI without FBS, then washed with RPMI containing 10% FBS. In some experiments, labeled B or $CD4^+$ T cells were incubated with the anti-mouse $\alpha_4\beta_7$ antibody DATK32[50] (50 μg/mL) in RPMI containing 10% FBS for 45 min at 37°C. Cells were washed three times to remove unbound antibodies. Prior to injection into recipient mice, cells were counted by flow cytometry using counting beads. Recipient mice were anesthetized via intraperitoneal injection of ketamine and xylasine. One individual Peyer's patch of the SI was exteriorized and positioned for epifluorescence microscopy and video recording. Same numbers (5-10 × 10^6 cells) of wild-type, *Cd22*$^{-/-}$, *Ptpn6*$^{+/meV}$ B or $CD4^+$ T cells were transferred into anesthetized recipients. The interactions of fluorescent cells with PP-HEVs were recorded for 30-40 sec at 40 frames per second of 25 msec exposure time. All fluorescent cells entering HEVs during the recording time were analyzed on a frame-to-frame basis for the entire duration of the movie. Cells passing HEVs <1 s with no significant interaction or with a velocity > 300 μm/s were considered noninteractive and called flyer; cells which started binding to HEVs briefly for <1s before getting releasing and non-interactive were considered as brief rollers. Cells binding to HEVs >1s were considered rollers. At the end of the recording, rollers attached to HEVs with a static binding of > 2s were considered arresters. To assess the mean rolling velocity of each cell, we tracked manually each cells using Imaris (version 9) to define the precise rolling distance from the frame of its first interaction (ffirst) to the first frame of its definitive static binding (f_{last}). The rolling time was (f_{last} – ffirst + 1) × 25 ms.

Short-term homing assay

Donor splenocytes were isolated and were labeled with Cell Trace Violet (CTV, Invitrogen) or CFSE (Invitrogen) in complete RPMI medium, or a combination of CTV and CFSE at concentrations optimized for a bar coding system with 2– 4 donor populations total. Equal numbers (25–50 × 10^6 cells) of donor cells were transferred into wild-type recipient mice by injection into the tail vein. After 1.5 h, lymphocytes from the PLNs and PPs (average of 5 PPs per mouse) of recipient mice were isolated, stained for flow cytometry to identify T and B cells (see **Integrin Expression by flow cytometry**). The LIVE/DEAD Fixable Aqua dye was used for live/dead staining and counting beads were added to calculate absolute cell numbers. The efficiency of B and T cell homing to each organ was calculated as a ratio: the number of cells found in each organ was divided by the number of cells injected (input). Then, results were presented as a percentage of the wild-type C57BL/6 (control group) mean ratio.

Proximity Ligation Assay (PLA)

B cells were isolated from wild-type and *Cd22*$^{-/-}$ splenocytes using negative selection kits. In some experiments, B cells were pre-treated with *Arthrobacter Uereafaciens* sialidase (Roche) at 125 mU/mL to remove α2-6 Sia modifications. Vehicle control treated (PBS) or

Europe PMC Funders Author Manuscripts

Europe PMC Funders Author Manuscripts

sialidase-treated purified B cells were cytospun on to a 1 cm^2 area of a slide at a concentration of 1.5×10^5/100 μL for 7 min at 700 rpm in the Cyto-Tek Centrifuge (Model No. 4324). The cell sections were fixed using 4% PFA for 5 min at 4°C, followed by washing with PBS three times. All subsequent incubations were carried out in a humidity chamber at 37°C following the Duolink Proximity Ligation assay kit (Sigma) instructions. The following combination of primary antibodies used were: mouse anti-mouse CD22 (Cy34.1) and goat anti-mouse β_7 or goat anti-mouse β_1; and goat anti-mouse β_1 and rat anti-mouse α_4 (PS/2) followed by In Situ PLA Probe Anti-Mouse MINUS and Anti-Goat PLUS (Sigma). At the end of the PLA procedure, the sections were stained with DAPI for the identification of nuclei. Images were captured on a Zeiss LSM 880 confocal microscope using the Zeiss Zen software, a 63× oil-immersion objective and 1.5× digital zoom. The number of PLA spots per image were quantified using Imaris (v.2.0.0-rc-49/1.51d).

Cellular localization of integrin β_7, CD22 and Shp1 by microscopy

B cells were isolated from wild-type and *Cd22*$^{-/-}$ splenocytes using negative selection kits. In some experiments, cells were stained with MitoTracker™ Deep Red FM (Invitrogen) at 0.5 μM for 15 min at 37°C to identify the cytoplasm. Cells were fixed using 1% PFA (Invitrogen) in PBS for 5 min at 4°C, then stained for extracellular β_7 and CD22 with goat anti-mouse β_7 and biotin mouse anti-mouse CD22 respectively in PBS for 40 min at 4°C, followed by Alexa Fluor 488-conjugated donkey anti-goat (for β_7) and Alexa Fluor 594-conjugated streptavidin (for CD22) for 40 min at 4°C. In some experiments, cells were permeabilized in 1× permeabilization buffer (PB) from Invitrogen for 30 min at 4°C after fixation, stained for Shp1, β_7, and CD22 with rabbit anti-human/mouse Shp1, goat anti-mouse β_7 and biotin mouse anti-mouse CD22 respectively in 1× PB for 60 min at 4°C, washed with fresh 1× PB, then stained with Alexa Fluor 594-conjugated donkey anti-rabbit (for Shp1), Alexa Fluor 488 donkey anti-goat (for β_7), and Alexa Fluor 647-conjugated streptavidin (for CD22). At the end of the staining procedure, cells were cytospun, stained with DAPI for the identification of nuclei, and images were captured as described above (see Proximity Ligation Assay). For each cell, we quantified the intensity of the β_7 fluorescence with ImageJ using the corrected total cell fluorescence. We counted manually the total number of β_7 spots at the cell surface found in close proximity with intracellular spots of Shp1 and expressed this number as a percentage of the total β_7 spots to yield a Shp1 – β_7 proximity index (%). Similarly, we counted the total number of CD22 spots at the cell surface found in close proximity to both β_7 and Shp1 and expressed this number as a percentage of the total β_7/Shp1 hotspots to yield a CD22 – Shp1/β_7 proximity index (%).

Endocytosis assay

Splenocytes were stained with fluorescently labeled antibodies against CD19, IgD and either CD71(TfR1), β_1, β_7, or the appropriate isotype control. The Fc receptors were blocked anti-CD16/32 prior to the staining. For each sample, staining at 4°C with Phycoerythrin (PE)-conjugated RI7217 (anti-Transferrin Receptor 1, TfR1), HMβ1-1 (anti-β_1), FIB504 (anti-β_7), or the matching PE-conjugated isotype control antibodies allowed calculation for extra-cellular amounts of TfR1, β_1, α_L, and β_7 concentrations. We used pHrodo™ iFL microscale protein labeling kits (Invitrogen) to label the antibody clones HMβ1-1, FIB504 or isotype-matched controls. In parallel, staining of each sample with pHrodo-Red-conjugated

Europe PMC Funders Author Manuscripts

Europe PMC Funders Author Manuscripts

Transferrin (Invitrogen), HMβ1-1, FIB504, or Isotype control antibodies at either 4°C (no endocytosis) or 37°C (endocytosis) for one hour was used to calculate endocytosis efficiency. The same staining protocol was performed in the presence of 100 μM Primaquine (PQ). Samples were analyzed by flow cytometry. For each antigen and each experiment, the Relative Endocytosis Ratio (RER) was calculated by normalizing endocytosis levels to extra-cellular levels, i.e.:

$$\mathrm{RER\ (of\ Antigen\ A)} = \frac{\mathrm{MFI\ Anti\text{-}A\text{-}PHrodo\text{-}Red\ Staining\ at\ 37°C\text{-}MFI\ Anti\text{-}A\text{-}PHrodo\text{-}Red\ staining\ at\ 4°C}}{\mathrm{MFI\ Anti\text{-}A\ PE\ staining\ at\ 4°C\text{-}MFI\ Isotype\ Control\text{-}PE\ staining\ at\ 4°C}}$$

Double immunoprecipitation (IP) and immunoblotting

Purified B or T cells were labeled with EZ-Link Sulfo-NHS-Biotin (Invitrogen) on ice for 60 min. Biotinylated cells were washed with HBSS and lysed in IP buffer (50 mM Tris-HCl pH 7.5 (Sigma); 150 mM NaCl (Sgma); 1% Triton × 100 (Sigma); 0.1% Na-deoxycholate (Sigma); 1 mM EDTA (Invitrogen); Complete Mini EDTA-free Protease inhibitors (Roche); and Phosphatase Inhibitor Cocktail 2 and 3 (Sigma) used at 1:100 dilution from stock) for 20 min on ice. Cell lysates were cleared from debris by centrifugation (16 000 × g, 10min, 4°C). After pre-clearing the lysates with unbound Dynabeads protein G beads (Invitrogen), β_7 integrin was pulled down by incubation of lysates with Dynabeads protein G bound to rat anti-mouse β_7 antibody FIB504[51] for overnight with agitation. After several washes with IP buffer, the β_7 integrin was eluted with 100 mM glycine buffer at pH 2.5 for 15 min at 56°C with gentle agitation. The acidic pH of the eluate was then quenched with two volumes of 100mM Tris-HCl pH 8.0. Biotinylated β_7 was pulled down from these eluates with SoftLink™ Soft Release Avidin Resin (Promega) overnight with agitation. The flow through of the streptavidin IP was spun in with 30 kDa molecular weight cutoff ultrafiltration tubes to concentrate the biotin-free β_7 fraction, then reduced with at 95°C for 5 min with 1× Laemmli buffer (Biorad) containing 5% beta-mercaptoethanol (BME) (Sigma). After overnight incubation, the avidin resin was washed three times with Tris-buffered saline (Sigma) containing 0.01% Tween 20 (Sigma), and biotinylated β_7 was eluted with 1× Laemmli buffer containing 5% BME (95°C, 5min).

Reduced biotin-free and biotinylated β_7 were then subjected to SDS-Page and immunoblot analysis. Integrin β_7 was detected from immunoblots with rat anti-mouse β_7 antibody (clone FIB504) plus HRP-conjugated goat anti-rat antibodies, followed by addition of the ECL substrate (Clarity™ Western ECL Substrate, Biorad). Blots were stripped (Restore™ PLUS Western Blot Stripping Buffer, Invitrogen) and tyrosine phosphorylation was detected with the mouse anti-phosphotyrosine antibody (clone PY20) plus HRP-conjugated goat anti-mouse followed by addition of the substrate. Images were captured using the Azure Biosystem 600 imaging system. Imaged blots were quantified using Image J.

Real-time quantitative RT-PCR

Total RNA was isolated from purified B cells using the RNeasy mini kit (Qiagen). Analysis of total RNA concentration and integrity was assessed using Nanodrop ND-1000 spectrophotometry. Equal amounts of each total RNA samples were converted into cDNA

Europe PMC Funders Author Manuscripts

Europe PMC Funders Author Manuscripts

using the High Capacity cDNA Reverse Transcription Kit (Invitrogen) according to the manufacturer's instructions. Quantitative RT-PCR analysis of genes of interest was performed using SYBR Green on a ABI PRISM® 7900HT (Applied Biosystems). PCR reaction mixtures consisted of: 1 μL of a 1:5 dilution of template cDNA, 200 nM of each primer, and 1× PowerSYBR® Green PCR Master Mix (Invitrogen) in a final volume of 10 μL. RT-qPCR amplication was conducted using an initial step of 5 min at 45°C, then 5 min at 95°C, followed by 40 cycles of denaturation at 95°C for 30 sec, primer annealing at 60°C for 30 sec, and extension at 72°C for 30 sec. Melting curve analysis was used to assess the purity of the amplified bands. Sequences for the primer pairs used for *Itgal*[52], *Itgb1*[52], *Itgb2*[52], *Itgb7*[53], and *Hprt*[54] are listed in Supplementary Table 2. Primer pairs for *Actb* were pre-designed from Qiagen. We used the $2^{-\Delta\Delta Ct}$ method to calculate the relative gene mRNA expression of *Itgal*, *Itgb1*, *Itgb2*, and *Itgb7* using *Actb* and *Hprt* as housekeeping genes.

CTB immunization studies

Adults C57BL/6 or *Cd22*$^{-/-}$ mice were immunized with 10 μg Cholera Toxin B (Sigma) diluted in 100 μL PBS for oral gavage (Oral route), 10 μL PBS for intranasal via pipetting in the nostrils (Nasal route), or 50 μL PBS for injection into the mouse hamstring (Muscular route). Mice were sacrificed two weeks post immunizations. Serum was collected for ELISA studies, and segments of SI used in *ex vivo* cultures.

Rotavirus infection studies

Five days old C57BL/6 or *Cd22*$^{-/-}$ pups were orally gavaged with 10^4 diarrhea dose 50% (DD_{50}) of wild-type murine rotavirus, strain EW, diluted in M199 medium. Pups were then checked daily for diarrhea by gentle abdominal pressure. Fecal samples from each individual mouse were collected in PBS with Calcium/Magnesium for enzyme-linked immunosorbent assays (ELISAs). In some studies, mice were sacrificed either at day 12 p.i. to collect the serum for ELISA studies, MLNs, SI lamina propria (SI LP) and spleen for ELISPOT analysis, and segments of SI for *ex vivo* cultures.

Detection of viral antigen and virus specific IgA and IgG by ELISA

For detection of viral antigen in fecal samples[55], 96-well ELISA plates were coated with guinea pig anti-rotavirus hyperimmune serum in PBS and incubated at 37°C for 4 h. The plates were then blocked with 5% non-fat milk in PBS (Blotto) at 37°C for 2 h. Suspended fecal samples were diluted 1:20 in 1% Blotto, added to the plates, and incubated at 37°C for 1 h. The plates were washed three times with PBS containing 0.05% Tween 20 (PBS-T). Rabbit anti-rotavirus hyperimmune serum (RARHS) in 1% Blotto was added to the plates for 1 h at 37°C, and washed three times. Horseradish peroxidase-conjugated goat anti-rabbit IgG in 1% Blotto was added to the plates and incubated for 1 h at 37°C. TMB substrate (Sigma) was added after four washes in PBS-T, the plates were developed for 10 min at room temperature, the reaction was stopped by the addition of 0.16 M sulfuric acid, and the OD450 read with a plate reader. Data are presented as OD450-like numbers after normalization to stools weight.

Europe PMC Funders Author Manuscripts

Europe PMC Funders Author Manuscripts

For the detection of virus-specific fecal and serum IgA and IgG, plates were coated with RARHS and blocked as described above, and then incubated with 1:5 of rotavirus stock (gift from H. Greenberg, Stanford University) in 1% Blotto overnight at 4°C. After three washes with PBS-T, stool samples (1:20 in Blotto) or serial dilutions of serum in 1% Blotto were added to the plates. After 2 h of incubation at 37°C, the plates were washed three times in PBS-T and peroxidase-conjugated anti-mouse IgA or IgG were added for 1 h at 37°C. Plates were washed and developed as described above. For the detection of total fecal and serum IgA or IgG, plates were coated with anti-mouse IgA, IgG, IgM polyclonal antibodies before using the same protocol as above.

Detection of CTB-specific IgA and IgG by ELISA

ELISA plates were coated with CTB (2 μg/mL) overnight, blocked with in PBS containing 5% BSA, then incubated with serial dilutions of serum or *ex vivo* SI culture samples diluted in PBS containing 2% BSA for 2 h. After four washes with PBS-T, peroxidase-conjugated anti-mouse IgA or IgG in 2% BSA were added for 1 h at 37°C. TMB substrate was added after four washes in PBS-T, the plates were developed for 5-10 min at room temperature, the reaction was stopped by the addition of 0.16 M sulfuric acid, and the OD450 read with a plate reader. For the detection of serum and *ex vivo* SI culture samples IgA or IgG, plates were coated with anti-mouse IgA, IgG, IgM polyconal antibodies before using the same protocol as above.

SI fragment cultures

Open segments (1 cm long) of duodenums were weighted and placed in 24-well plates on elevated mesh filter and cultured for three days at 37°C in complete RPMI medium in hyper oxygenated conditions[56]. At the end of the incubation period, intestinal IgA and IgG were measured by ELISA in the supernatants as described above.

Quantitation of virus-specific antibody secreting cells (ASCs) by Elispot assay

Multiscreen 96-well plates (MAIPS4510, Millipore) were coated with purified rotavirus double-layer particle (gift from H. Greenberg) overnight at 4°C, washed, and blocked with RPMI medium containing 10% FCS for 1 h at 37°C. Serial 10-fold dilutions of spleen, PP, or SI LP cells were added to the plates, and incubated overnight at 37°C. After six washes, peroxidase-conjugated anti-mouse IgA or IgG were added for 1 h at 37°C. Plates were washed six times and developed with AEC substrate (Vector Laboratories). To quantity non-specific ASCs, plates were coated with anti-mouse IgA, IgG, IgM polyclonal antibodies before using the same protocol as above.

Statistical analyses

All data were organized in Microsoft Excel (v16.42) spreadsheets and we performed all our statistical analyses using GraphPad Prism (v8.4.1). For each data set shown and analyzed, the test used is indicated in the figure legend. Statistical significance is indicated by the following: $*P \leq 0.05$, $**P \leq 0.01$, $***P \leq 0.001$ and $****P \leq 0.0001$. No statistical significance is indicated with ‘ns’.

Europe PMC Funders Author Manuscripts

Europe PMC Funders Author Manuscripts

Reporting Summary

Further information on research design is available in the Nature Research Reporting Summary linked to this article.

Extended Data

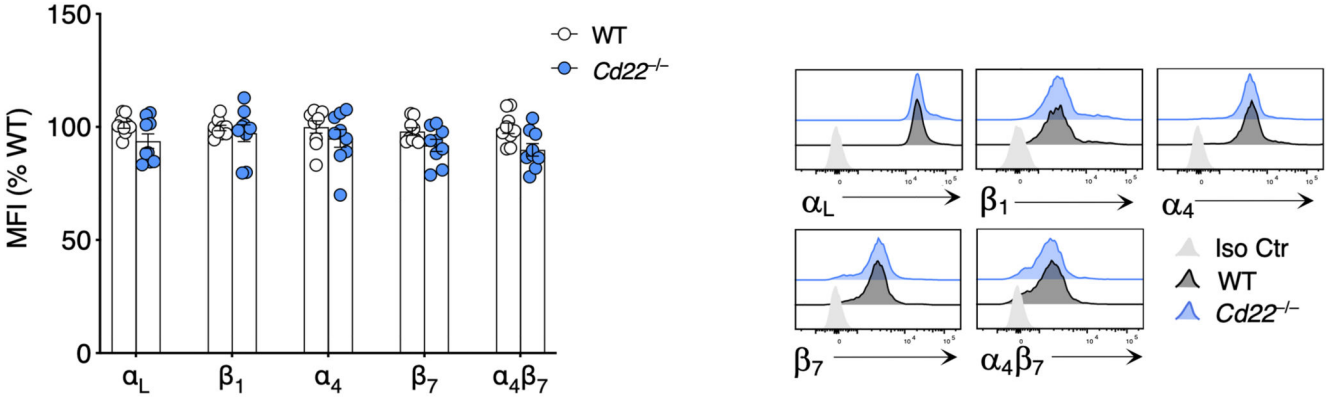

Extended Data Fig. 1. CD22-deficient T cells display normal cell surface levels of $\alpha_4\beta_7$.

Flow cytometry of WT or *Cd22*$^{-/-}$ live CD3$^+$ CD4$^+$ T cells isolated from spleens and stained with antibodies against the integrins α_L, β_1, α_4, β_7, or $\alpha_4\beta_7$. Shown are pooled data (mean ± SEM) from n=3 independent experiments with 7 animals per group total presented as in Figure 1. Representative histogram overlays gated in CD4$^+$ T cells are shown.

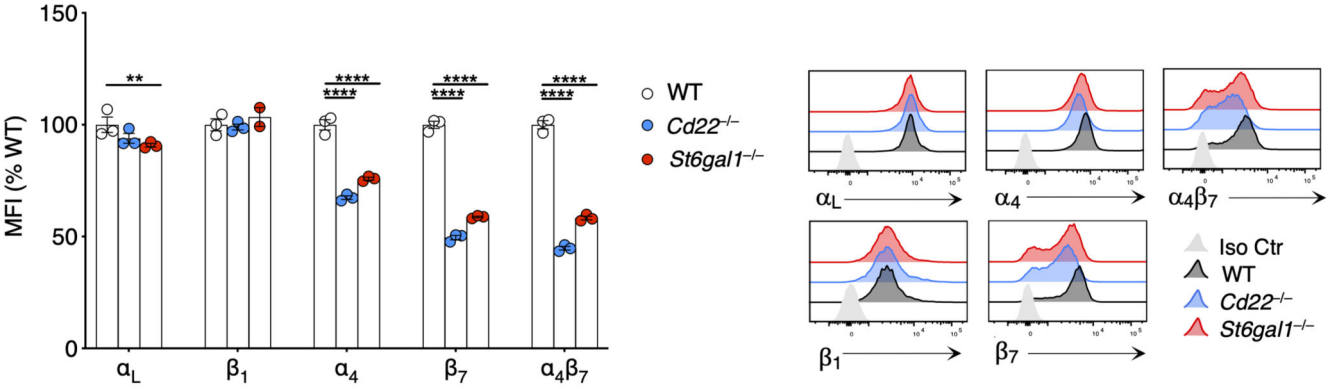

Extended Data Fig. 2. B cell expression of St6gal1-dependent CD22-binding carbohydrates controls $\alpha_4\beta_7$ expression.

Flow cytometry of WT, *Cd22*$^{-/-}$, or *St6Gal1*$^{-/-}$ naïve B cell (CD19$^+$ IgD$^+$) isolated from spleen and stained with antibodies against the integrins α_L, β_1, α_4, β_7, or $\alpha_4\beta_7$. Data represent the mean ± SEM of one representative experiment with n=3 mice per group presented as in Figure 1. Representative histogram overlays gated in naïve B cells are shown. Groups were compared using One-way ANOVA with Dunnett's multiple comparisons test. **P ≤ 0.01, and ****P≤0.0001

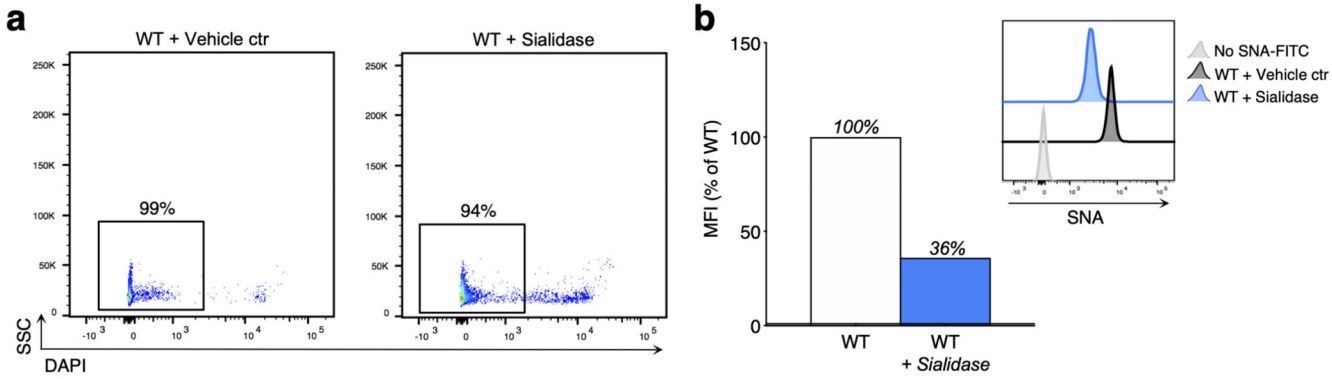

Extended Data Fig. 3. Removal of α2-6 Sia linkages on B cells with *Arthrobacter Uereafaciens* sialidase.

Purified wild type B cells purified from spleen were incubated for one hour at 37 °C with *Arthrobacter ureafaciens* sialidase or with vehicle control (PBS, Vehicle Ctr). **a,b**, Flow cytometry of *Arthrobacter ureafaciens-treated* or vehicle control-treated WT naïve B cells (CD19+ IgD+), isolated from spleen and stained for DAPI and SNA-FITC. **a**, The percentage of viable cells is shown. **b**, The MFI of the SNA staining was expressed as a percentage of the mean MFI of the vehicle ctr-treated WT B cell group. Representative histogram overlay gated in live naïve B cells is shown.

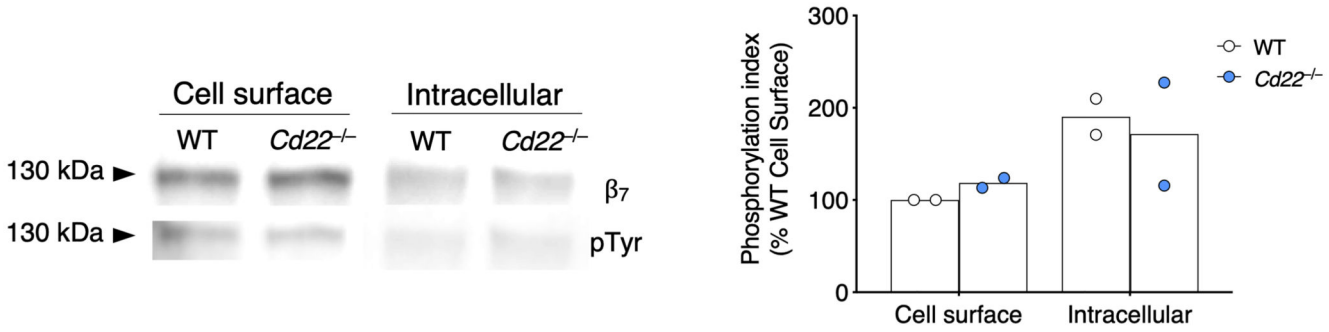

Extended Data Fig. 4. CD22-deficient T cells display wild-type levels of tyrosine phosphorylation in cell surface β7.

Left panel: detection of β_7 and phosphotyrosine (pTyr) levels in the cell surface and intracellular β_7 fractions of wild-type (WT) and CD22-deficient (*Cd22*$^{-/-}$) T cells after the double IP as shown in Fig. 5a. Right panel: quantification of pTyr levels normalized to β_7 levels (pTyr/β_7 ratio). Within each experiment, the pTyr/β_7 of the cell surface β_7 of the WT group was set to 100, and data expressed as a percentage of this total. Each dot represents one independent experiment with n=4 animals pooled for WT and *Cd22*$^{-/-}$ (i.e. n=8 animals total for the two experimental replicates).

Europe PMC Funders Author Manuscripts
Europe PMC Funders Author Manuscripts

Europe PMC Funders Author Manuscripts

Europe PMC Funders Author Manuscripts

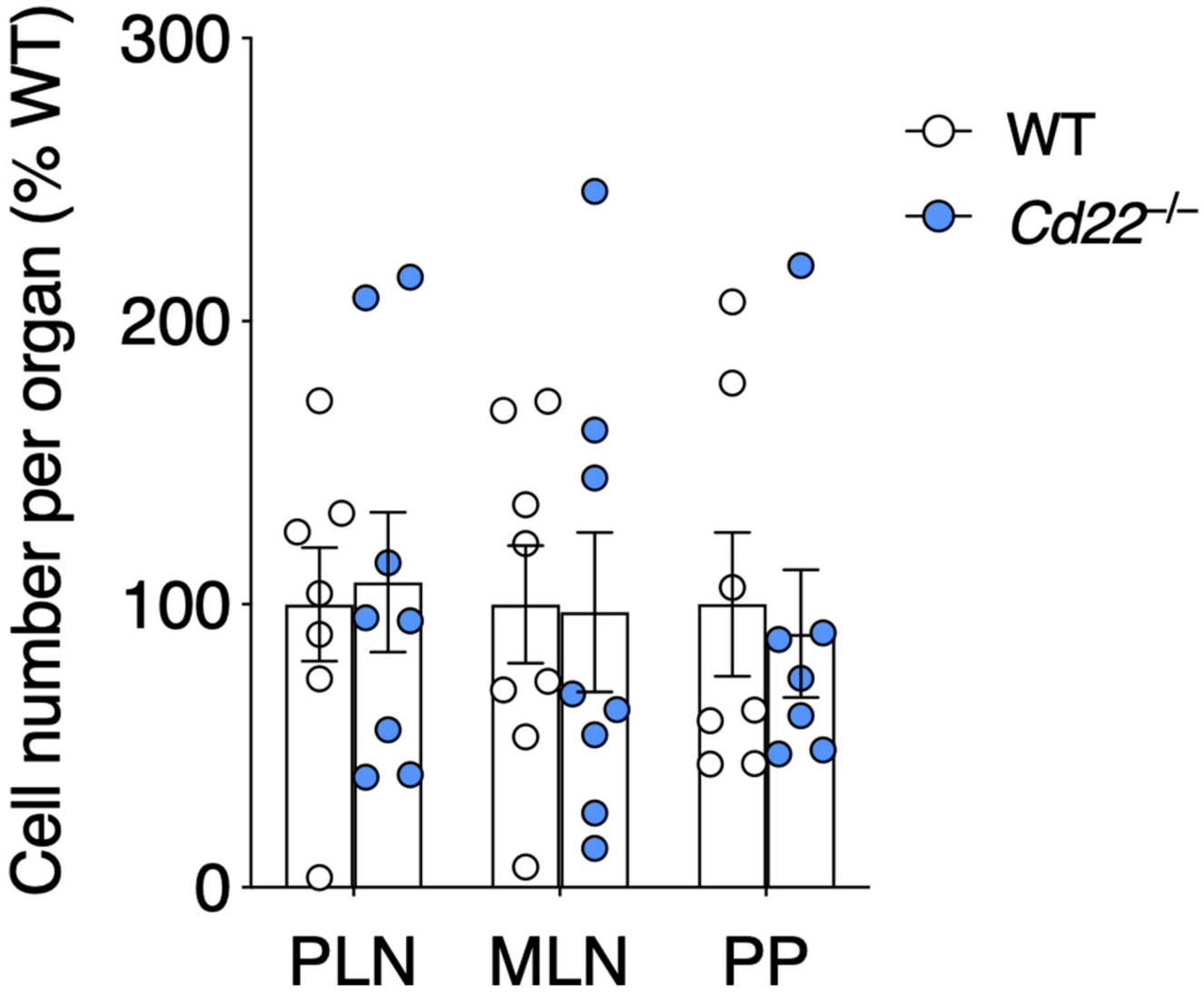

Extended Data Fig. 5. Normal T cell numbers in CD22-deficient Peyer's patches and lymph nodes.

Numbers of $CD4^+$ T cells ($CD3^+$ $CD4^+$) in MLN, PLN, and PP of WT and *Cd22*$^{-/-}$ shown as a percentage of the mean of the WT group. Shown are pooled data (mean ± SEM) of n=2 experiments with n=7-8 mice per group total.

Europe PMC Funders Author Manuscripts

Europe PMC Funders Author Manuscripts

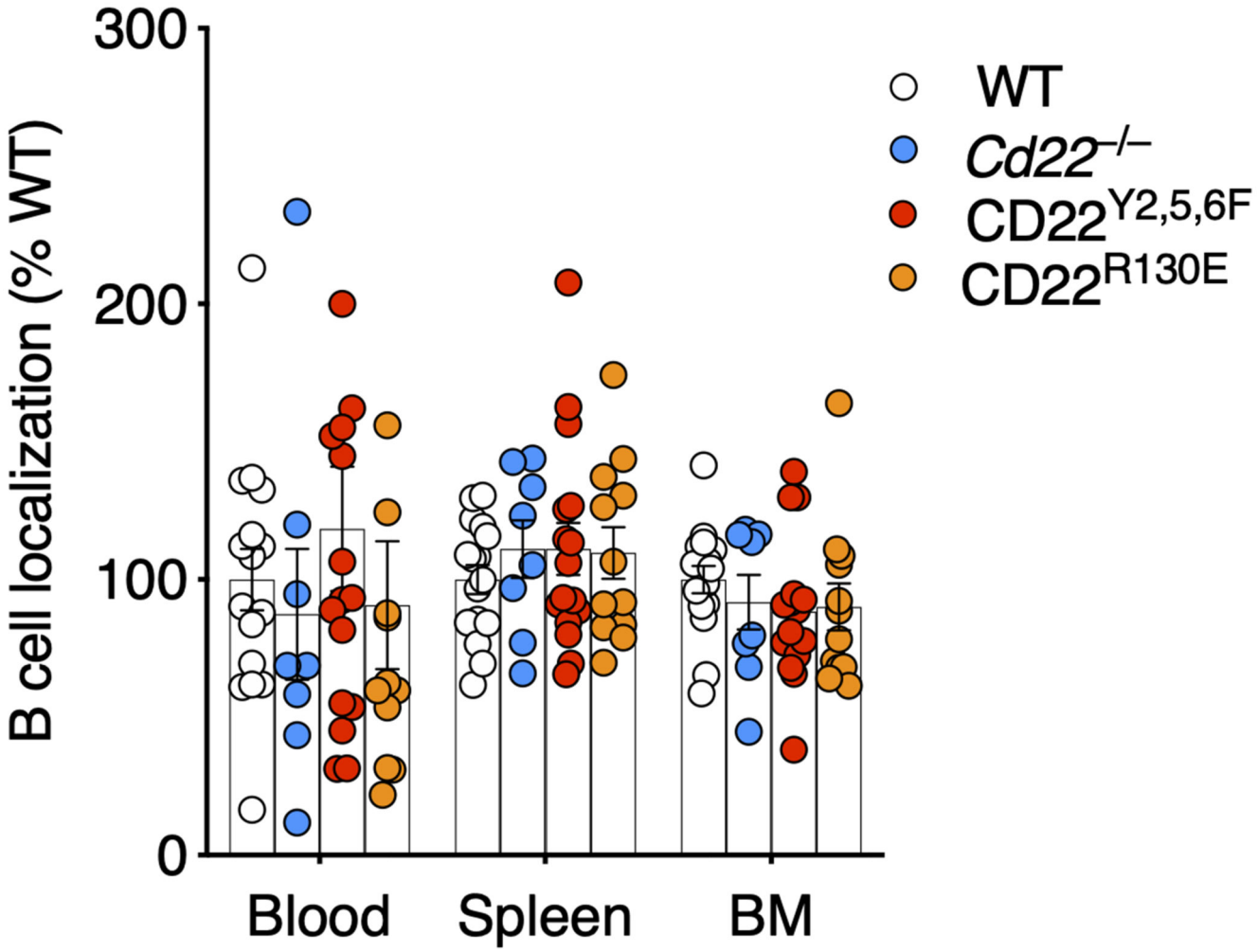

Extended Data Fig. 6. Functional assays reveal normal homing of CD22 mutant B cells to the spleen and bone marrow.

Localization of WT, *Cd22* $^{-/-}$, CD22^{Y2,5,6F}, and CD22^{R130E} B cells in blood, spleen and bone marrow (BM) after homing assays as illustrated in Fig. 6c. Data are shown as a percentage of the mean localization ratio of the WT group. Shown are pooled data (mean ± SEM) of n=3-5 experiments with 11-16 mice per group total.

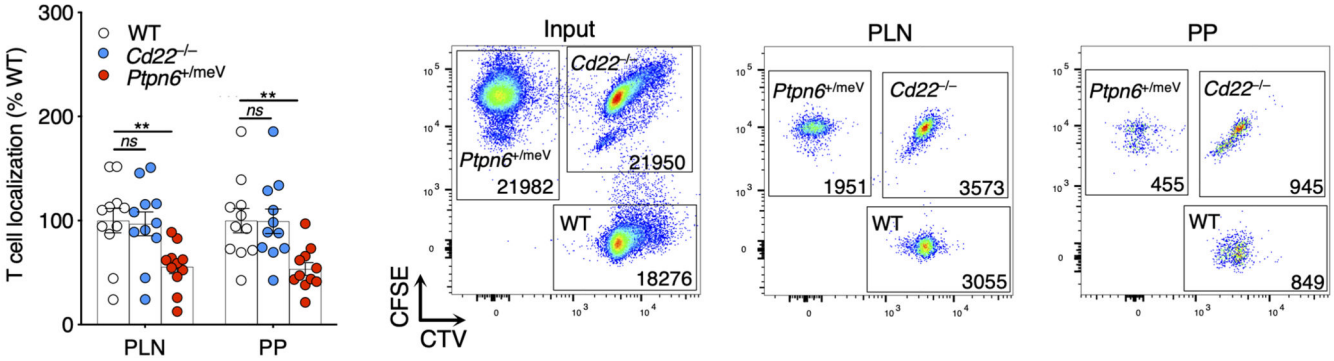

Extended Data Fig. 7. Localization of WT, *Cd22* $^{-/-}$, and *Ptpn6* $^{+/meV}$ T cells in PLN and PP after short-term homing assays.

WT, *Cd22* $^{-/-}$, or *Ptpn6* $^{+/meV}$ splenocytes labeled with CFSE, or CellTracker Violet (CTV) or both were injected i.v. into a recipient WT mouse. PLN, MLN or PP cells isolated from the recipient were stained with anti-CD3 and anti-CD4 for quantification of short-term (90 min) homing of CD4 T cells. For each donor and each organ, the number of isolated CD4 T cells (Output) was normalized to the number of injected CD4 T cells (Input) to yield a T cell localization ratio. Shown is the mean ± SEM from three independent experiments with n=11 mice per group total. Representative dot plots gated in live $CD3^+$ $CD4^+$ T cells are shown, including the number of cells within each gate. Groups were compared using One-way ANOVA with Dunnett's multiple comparison test. **P ≤ 0.01, and ns: not significant.

Europe PMC Funders Author Manuscripts
Europe PMC Funders Author Manuscripts

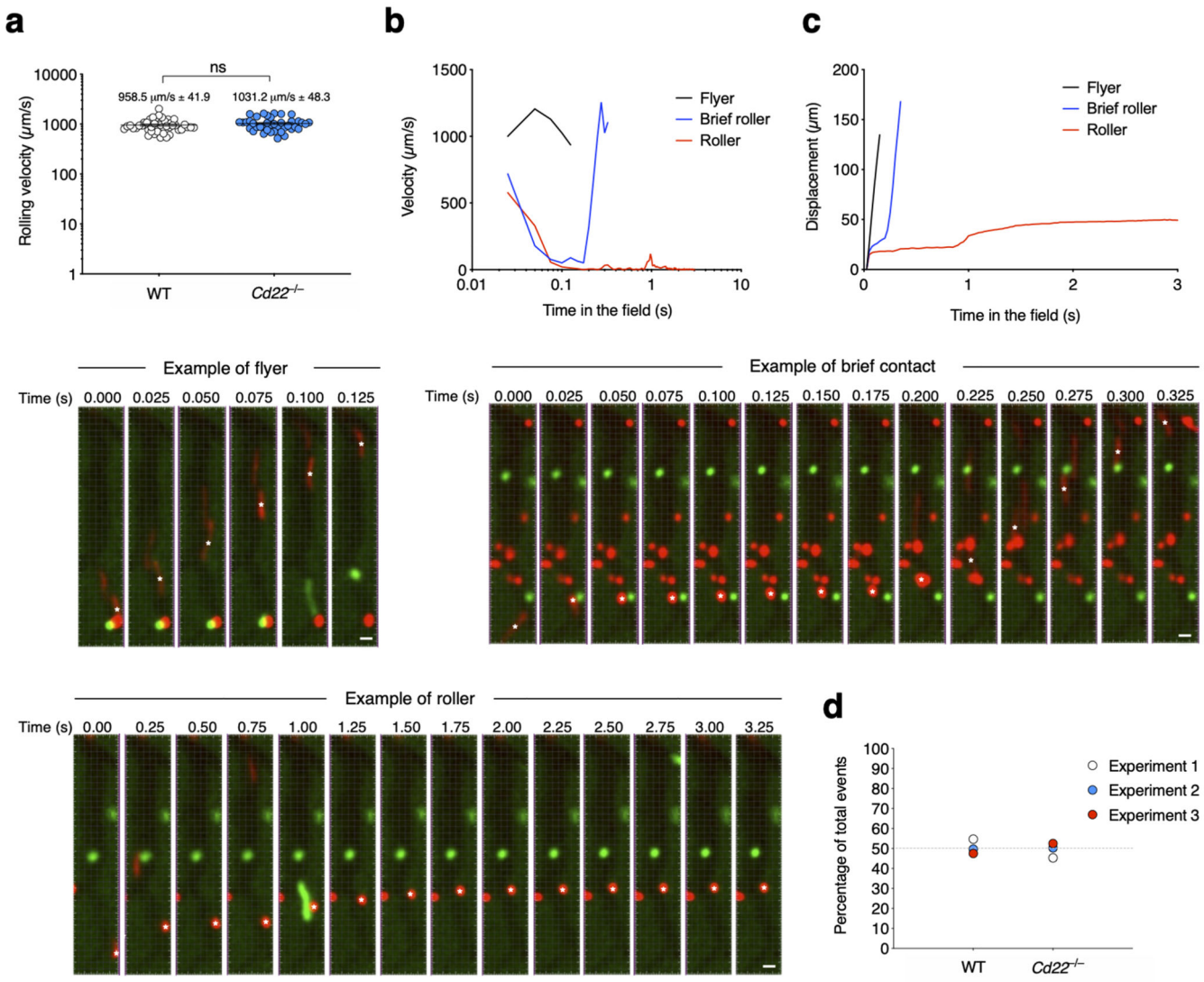

Extended Data Fig. 8. Definition of flyer, brief roller and roller cells visualized by *in situ* video microscopy of Peyer's patches.

a, The mean velocity of wild-type (WT) and CD22-deficient (*Cd22*$^{-/-}$) B cells free flowing through the vessels without any interactions (namely flyer) was calculated and shown for each individual cell. Shown are pooled results (~ 50 cells per group) analyzed from 3–4 representative HEVs and 3 independent experiments. **b,c**, The instant velocity (b) and displacement (c) of a representative free flowing cell (Flyer), of one that interacts very briefly (<1s) with the HEVs (namely Brief roller), or one that interacts and rolls on the HEVs for >1sec (namely Roller) is shown together with frame-per-frame tracking of the cells (identified with *). Scale bars: 10 µm. **d**, In three independent *in situ* experiments with 1:1 ratio of WT B cells donor versus *Cd22*$^{-/-}$ B cells donor, the total number of events (i.e. flyer, brief roller, or roller) was counted for each donor in 3–4 representative HEVs for the total duration of the movie (~ 250–300 total cells analyzed per group). The percentage of WT and *Cd22*$^{-/-}$ B cells experiment per experiment is shown. ns: not significant.

Europe PMC Funders Author Manuscripts
Europe PMC Funders Author Manuscripts

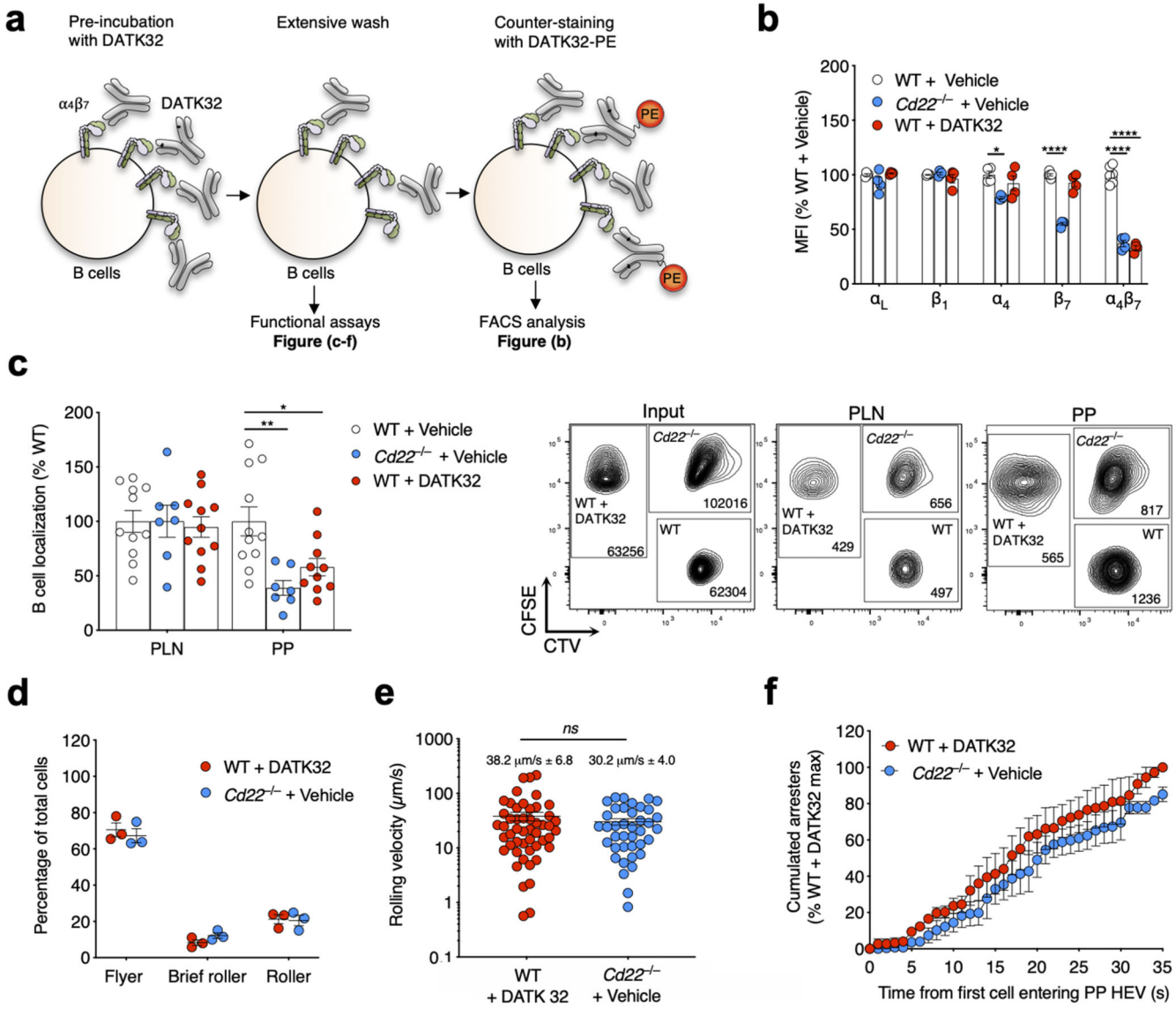

Extended Data Fig. 9. WT B cells with reduced $\alpha_4\beta_7$availability mimic the behavior of defective CD22-deficient B cell homing to PP.

a, WT B cells were pre-incubated with inhibitory anti-$\alpha_4\beta_7$ Ab DATK32 (50 μg/mL) and washed extensively. DATK32-pretreated B cells were either counter-stained with Phyco-erythrin(PE)-conjugated DATK32 for flow cytometry analyses (b), or use in functional assays (c-f). **b**, Flow cytometry of WT + DATK32 vs. WT + Vehicle B cells stained for α_L, β_1, α_4, β_7, or $\alpha_4\beta_7$ presented as in Figure 1. Shown are pooled data (mean ± SEM) from n=2 independent experiments with 4 animals per group total. **(c)** Localization of WT, *Cd22* $^{-/-}$, and WT + DATK32 B cells in PLN and PP after homing assays analyzed and presented as in Figure 6. Shown are pooled data (mean ± SEM) of n=3 experiments with 11 mice per group total. Representative dot plots gated in live naïve B cells are also shown including the number of cells within each gate. **d-f**, *In situ* video microscopy analyses of WT B cells + DATK32 vs. *Cd22* $^{-/-}$ B cells interactions with PP-HEVs analyzed and presented as in Figure 6. Data represent the mean ± SEM of three independent experiments (d,f) and

Europe PMC Funders Author Manuscripts
Europe PMC Funders Author Manuscripts

representative cells from all 3 experiments (e). Groups were compared using One-way ANOVA with Dunnett's multiple comparisons test (b,c), unpaired two-tailed Student's *t*-test (d,e), and paired two-tailed Student's t-test (f). *P ≤ 0.05, **P ≤ 0.01, and ****P≤0.0001. ns: not significant.

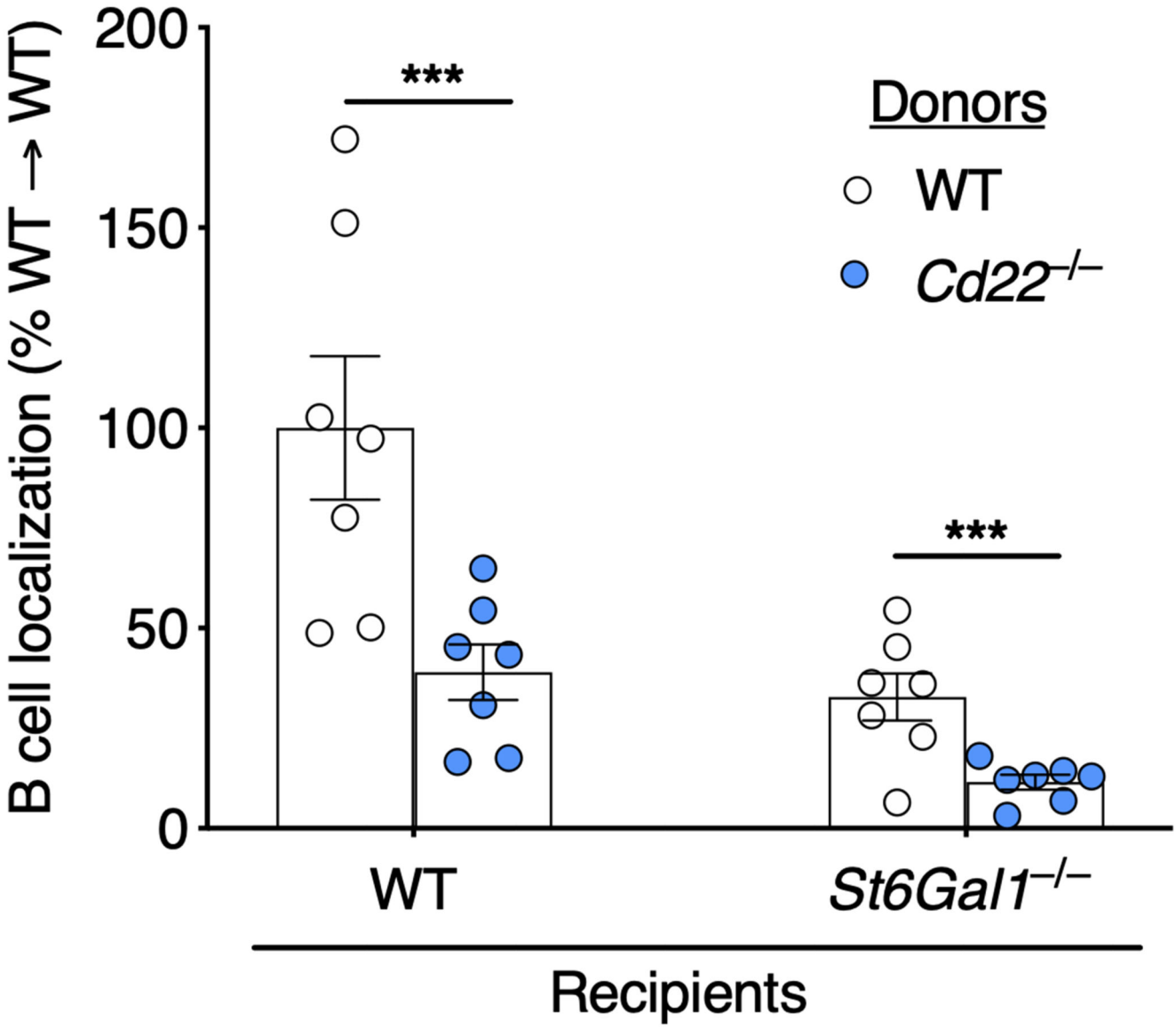

Extended Data Fig. 10. Defective homing of CD22-deficient B cells in St6gal1-deficient recipient mice.

Localization of WT and *Cd22*$^{-/-}$ B cells in the PPs of wild-type (WT) or ligand-deficient (*St6Gal1*$^{-/-}$) mice after short-term (1.5 hr) homing assays designed as in Figure 6a. For each donor, the number of B cells isolated (Output) was normalized to the number of injected B cells (Input) and shown as a percentage of the WT → WT group mean. Shown are pooled data (mean ± SEM) from three experiments with n=7 mice per group total. Groups were compared using two-tailed Student's t-test. ***P ≤ 0.001.

Europe PMC Funders Author Manuscripts
Europe PMC Funders Author Manuscripts

Europe PMC Funders Author Manuscripts

Europe PMC Funders Author Manuscripts

Supplementary Material

Refer to Web version on PubMed Central for supplementary material.

Acknowledgements

We thank J. Paulson from the The Scripps Research Institute for the *Cd22*$^{-/-}$ and *St6gal1*$^{-/-}$ mice; the members of the Butcher lab for discussions; J. Pan for help in designing primers; H. Hadeiba and A. Scholz for helpful discussions; C. Garzon-Coral for designing and making re-usable dishes used for positioning animals in intravital imaging studies; J.L. Jang for the production of home-made Abs used in these studies; M. Bscheider for helping implementing the imaging softwares in the Butcher lab that were used to record and analyzed the video microscopy; M. Lajevic for sharing protocols and expertise. This work was supported by NIH grants R37AI047822 and R01 AI130471 and award I01 BX-002919 from the Department of Veterans Affairs to E.C.B.; by the Swiss National Sciences Foundation grants P2GEP3_162055 and P300PA_174365 to R.B.; the DFG-funded TRR130 (project 04) to L.N.; JSPS Grant-in-Aid for Scientific Research 18H02610 and 19H04804 to T.T.; 1R01 AI125249 (NIH/NIAID), 1IO 1BX000158-01A1 (Veterans Affairs) to H.B.G.; and the Ramon Areces Foundation (Madrid, Spain) Postdoctoral Fellowship and Research Fellow Award (Crohn's and Colitis Foundation of America) to B.O. M.S.M. acknowledges funding provided through NIAID (AI118842).

Data availability

The data that support the findings of this study are available from the corresponding author upon request.

References

1. Berlin C, et al. α4β7 integrin mediates lymphocyte binding to the mucosal vascular addressin MAdCAM-1. Cell. 1993; 74:185–195. [PubMed: 7687523]
2. Bargatze RF, Jutila MA, Butcher EC. Distinct roles of L-selectin and integrins α4β7 and LFA-1 in lymphocyte homing to Peyer's patch-HEV in situ: The multistep model confirmed and refined. Immunity. 1995; 3:99–108. [PubMed: 7542550]
3. Streeter PR, Berg EL, Rouse BTN, Bargatze RF, Butcher EC. A tissue-specific endothelial cell molecule involved in lymphocyte homing. Nature. 1988; 331:41–46. [PubMed: 3340147]
4. Butcher EC, Williams M, Youngman K, Rott L, Briskin M. Lymphocyte trafficking and regional immunity. Adv Immunol. 1999; 72:209–253. [PubMed: 10361577]
5. Stevens SK, Weissman IL, Butcher EC. Differences in the migration of B and T lymphocytes: organ-selective localization in vivo and the role of lymphocyte-endothelial cell recognition. J Immunol. 1982; 128:844–851. [PubMed: 6976385]
6. Tang ML, Steeber DA, Zhang XQ, Tedder TF. Intrinsic differences in L-selectin expression levels affect T and B lymphocyte subset-specific recirculation pathways. J Immunol. 1998; 160:5113–5121. [PubMed: 9590263]
7. Green MC, Shultz LD. Motheaten, an immunodeficient mutant of the mouse: I. Genetics and pathology. J Hered. 1975; 66:250–258. [PubMed: 1184950]
8. Coman DREX, Bailey CL. 'Viable Motheaten,' a New Allele at the Motheaten Locus. Am J Pathol. 1984; 116:179–192. [PubMed: 6380298]
9. Neel BG, Gu H, Pao L. The 'Shp'ing news: SH2 domain-containing tyrosine phosphatases in cell signaling. Trends Biochem Sci. 2003; 28:284–293. [PubMed: 12826400]
10. Zhang J, Somani AK, Siminovitch KA. Roles of the SHP-1 tyrosine phosphatase in the negative regulation of cell signalling. Semin Immunol. 2000; 12:361–378. [PubMed: 10995583]
11. Sauer MG, Herbst J, Diekmann U, Rudd CE, Kardinal C. SHP-1 Acts as a Key Regulator of Alloresponses by Modulating LFA-1-Mediated Adhesion in Primary Murine T Cells. Mol Cell Biol. 2016; 36:3113–3127. [PubMed: 27697866]
12. Meyer SJ, Linder AT, Brandl C, Nitschke L. B Cell Siglecs-News on Signaling and Its Interplay With Ligand Binding. Front Immunol. 2018; 9:2820. [PubMed: 30559744]

Europe PMC Funders Author Manuscripts

13. Pao LI, et al. B Cell-Specific Deletion of Protein-Tyrosine Phosphatase Shp1 Promotes B-1a Cell Development and Causes Systemic Autoimmunity. Immunity. 2007; 27:35–48. [PubMed: 17600736]
14. Mercadante ER, Lorenz UM. T Cells Deficient in the Tyrosine Phosphatase SHP-1 Resist Suppression by Regulatory T Cells. J Immunol. 2017; 199:129–137. [PubMed: 28550200]
15. Martinez RJ, Morris AB, Neeld DK, Evavold BD. Targeted loss of SHP1 in murine thymocytes dampens TCR signaling late in selection. Eur J Immunol. 2016; 46:2103–2110. [PubMed: 27354309]
16. Müller J, et al. CD22 ligand-binding and signaling domains reciprocally regulate B-cell Ca2+ signaling. Proc Natl Acad Sci U S A. 2013; 110:12402–12407. [PubMed: 23836650]
17. Han S, Collins BE, Bengtson P, Paulson JC. Homomultimeric complexes of CD22 in B cells revealed by protein-glycan cross-linking. Nat Chem Biol. 2005; 1:93–97. [PubMed: 16408005]
18. Stamenkovic I, Sgroi D, Aruffo A, Sy MS, Anderson T. The B lymphocyte adhesion molecule CD22 interacts with leukocyte common antigen CD45RO on T cells and a2$\hat{\phi}$6 sialyltransferase, CD75, on B cells. Cell. 1991; 66:1133–1144. [PubMed: 1717156]
19. Gasparrini F, et al. Nanoscale organization and dynamics of the siglec CD22 cooperate with the cytoskeleton in restraining BCR signalling. EMBO J. 2015; 35:1–23. [PubMed: 26567170]
20. Hennet T, Chui D, Paulson JC, Marth JD. Immune regulation by the ST6Gal sialyltransferase. Proc Natl Acad Sci U S A. 1998; 95:4504–4509. [PubMed: 9539767]
21. Cullen PJ, Steinberg F. To degrade or not to degrade: mechanisms and significance of endocytic recycling. Nat Rev Mol Cell Biol. 2018; 19:679–696. [PubMed: 30194414]
22. Van Weert AWM, Geuze HJ, Groothuis B, Stoorvogel W. Primaquine interferes with membrane recycling from endosomes to the plasma membrane through a direct interaction with endosomes which does not involve neutralisation of endosomal pH nor osmotic swelling of endosomes. Eur J Cell Biol. 2000; 79:394–399. [PubMed: 10928454]
23. Legate KR, Fassler R. Mechanisms that regulate adaptor binding to ß-integrin cytoplasmic tails. J Cell Sci. 2008; 122:187–198.
24. Oxley CL, et al. An integrin phosphorylation switch: The effect of ß3 integrin tail phosphorylation on Dok1 and talin binding. J Biol Chem. 2008; 283:5420–5426. [PubMed: 18156175]
25. Calderwood DA, et al. Integrin ß cytoplasmic domain interactions with phosphotyrosine-binding domains: A structural prototype for diversity in integrin signaling. Proc Natl Acad Sci U S A. 2003; 100:2272–2277. [PubMed: 12606711]
26. Smith MJ, Hardy WR, Murphy JM, Jones N, Pawson T. Screening for PTB Domain Binding Partners and Ligand Specificity Using Proteome-Derived NPXY Peptide Arrays. Mol Cell Biol. 2006; 26:8461–8474. [PubMed: 16982700]
27. Anthis NJ, et al. B Integrin Tyrosine Phosphorylation Is a Conserved Mechanism for Regulating Talin-Induced Integrin Activation. J Biol Chem. 2009; 284:36700–36710. [PubMed: 19843520]
28. Caswell PT, Vadrevu S, Norman JC. Integrins: Masters and slaves of endocytic transport. Nat Rev Mol Cell Biol. 2009; 10:843–853. [PubMed: 19904298]
29. Butcher EC, Szabo MC, McEvoy LM. Specialization of Mucosal Follicular Dendritic Cells Revealed by Mucosal Addressin-Cell Adhesion Molecule-1 Display. J Immunol. 1997; 158:5584–5588. [PubMed: 9190904]
30. Altevogt P, et al. The alpha 4 integrin chain is a ligand for alpha 4 beta 7 and alpha 4 beta 1. J Exp Med. 1995; 182:345–355. [PubMed: 7629498]
31. Williams MB, et al. The memory B cell subset responsible for the secretory IgA response and protective humoral immunity to rotavirus expresses the intestinal homing receptor, alpha4beta7. J Immunol. 1998; 161:4227–4235. [PubMed: 9780197]
32. Habtezion A, Nguyen LP, Hadeiba H, Butcher EC. Leukocyte Trafficking to the Small Intestine and Colon. Gastroenterology. 2016; 150:340–354. [PubMed: 26551552]
33. Seong Y, et al. Trafficking receptor signatures define blood plasmablasts responding to tissue-specific immune challenge. JCI insight. 2017; 2:e90233. [PubMed: 28352656]
34. Franco MA, Greenberg HB. Immunity to rotavirus infection in mice. J Infect Dis. 1999; 179:466–469.

Europe PMC Funders Author Manuscripts

Europe PMC Funders Author Manuscripts

35. Anthis NJ, et al. β Integrin Integrin Tyrosine Phosphorylation Is a Conserved Mechanism for Regulating Talin-Induced Integrin Activation. J Biol Chem. 2009; 284:36700–36710. [PubMed: 19843520]
36. Tehran, Azarnia; Lòpez-HernándezMaritzen. Endocytic Adaptor Proteins in Health and Disease: Lessons from Model Organisms and Human Mutations. Cells. 2019; 8:1345.
37. Nishimura T, Kaibuchi K. Numb Controls Integrin Endocytosis for Directional Cell Migration with aPKC and PAR-3. Dev Cell. 2007; 13:15–28. [PubMed: 17609107]
38. Sun H, et al. Distinct chemokine signaling regulates integrin ligand specificity to dictate tissue-specific lymphocyte homing. Dev Cell. 2014; 30:61–70. [PubMed: 24954024]
39. Steinberg F, Heesom KJ, Bass MD, Cullen PJ. SNX17 protects integrins from degradation by sorting between lysosomal and recycling pathways. J Cell Biol. 2012; 197:219–230. [PubMed: 22492727]
40. Ghai R, et al. Structural basis for endosomal trafficking of diverse transmembrane cargos by PX-FERM proteins. Proc Natl Acad Sci U S A. 2013; 110:643–652.
41. Nitschke L, Carsetti R, Ocker B, Köhler G, Lamers MC. CD22 is a negative regulator of B-cell receptor signalling. Curr Biol. 1997; 7:133–143. [PubMed: 9016707]
42. Schippers A, et al. β7 integrin controls immunogenic and tolerogenic mucosal B cell responses. Clin Immunol. 2012; 144:87–97. [PubMed: 22710445]
43. Sato S, et al. CD22 is both a positive and negative regulator of B lymphocyte antigen receptor signal transduction: Altered signaling in CD22-deficient mice. Immunity. 1996; 5:551–562. [PubMed: 8986715]
44. Feng, N, Franco, MA, Greenberg, HB. Murine Model of Rotavirus InfectionMechanisms in the Pathogenesis of Enteric Diseases. Paul, PS, Francis, DH, Benfield, DA, editors. Springer; US: 1997. 233–240.
45. Marcelin G, Miller AD, Blutt SE, Conner ME. Immune Mediators of Rotavirus Antigenemia Clearance in Mice. J Virol. 2011; 85:7937–7941. [PubMed: 21593155]
46. Blutt SE, Miller AD, Salmon SL, Metzger DW, Conner ME. IgA is important for clearance and critical for protection from rotavirus infection. Mucosal Immunol. 2012; 5:712–719. [PubMed: 22739233]
47. Lopatin U, Blutt SE, Conner ME, Kelsall BL. Lymphotoxin Alpha-Deficient Mice Clear Persistent Rotavirus Infection after Local Generation of Mucosal IgA. J Virol. 2012; 87:524–530. [PubMed: 23097456]
48. Lee M, et al. Transcriptional programs of lymphoid tissue capillary and high endothelium reveal control mechanisms for lymphocyte homing. Nat Immunol. 2014; 15:982–795. [PubMed: 25173345]
49. Goswami D, et al. Endothelial CD99 supports arrest of mouse neutrophils in venules and binds to neutrophil PILRs. Blood. 2017; 129:1811–1822. [PubMed: 28223280]
50. Hamann A, Andrew DP, Jablonski-Westrich D, Holzmann B, Butcher EC. Role of alpha 4-integrins in lymphocyte homing to mucosal tissues in vivo. J Immunol. 1994; 152:3282–3293. [PubMed: 7511642]
51. Andrew DP, et al. Distinct but overlapping epitopes are involved in alpha 4 beta 7-mediated adhesion to vascular cell adhesion molecule-1, mucosal addressin-1, fibronectin, and lymphocyte aggregation. J Immunol. 1994; 153:3847. [PubMed: 7523506]
52. DeNucci CC, Pagán AJ, Mitchell JS, Shimizu Y. Control of a4β7 Integrin Expression and CD4 T Cell Homing by the β1 Integrin Subunit. J Immunol. 2010; 184:2458–2467. [PubMed: 20118278]
53. Eun JP, et al. Aberrant activation of integrin a4β7 suppresses lymphocyte migration to the gut. J Clin Invest. 2007; 117:2526–2538. [PubMed: 17786243]
54. Ocón B, et al. The glucocorticoid budesonide has protective and deleterious effects in experimental colitis in mice. Biochem Pharmacol. 2016; 116:73–88. [PubMed: 27431777]
55. Franco MA, Greenberg HB. Role of B Cells and Cytotoxic T Lymphocytes in Clearance of and Immunity to Rotavirus Infection in Mice. J Virol. 1995; 69:7800–7806. [PubMed: 7494291]
56. Feng N, et al. Redundant Role of Chemokines CCL25/TECK and CCL28/MEC in IgA + Plasmablast Recruitment to the Intestinal Lamina Propria After Rotavirus Infection. J Immunol. 2006; 176:5749–5759. [PubMed: 16670280]

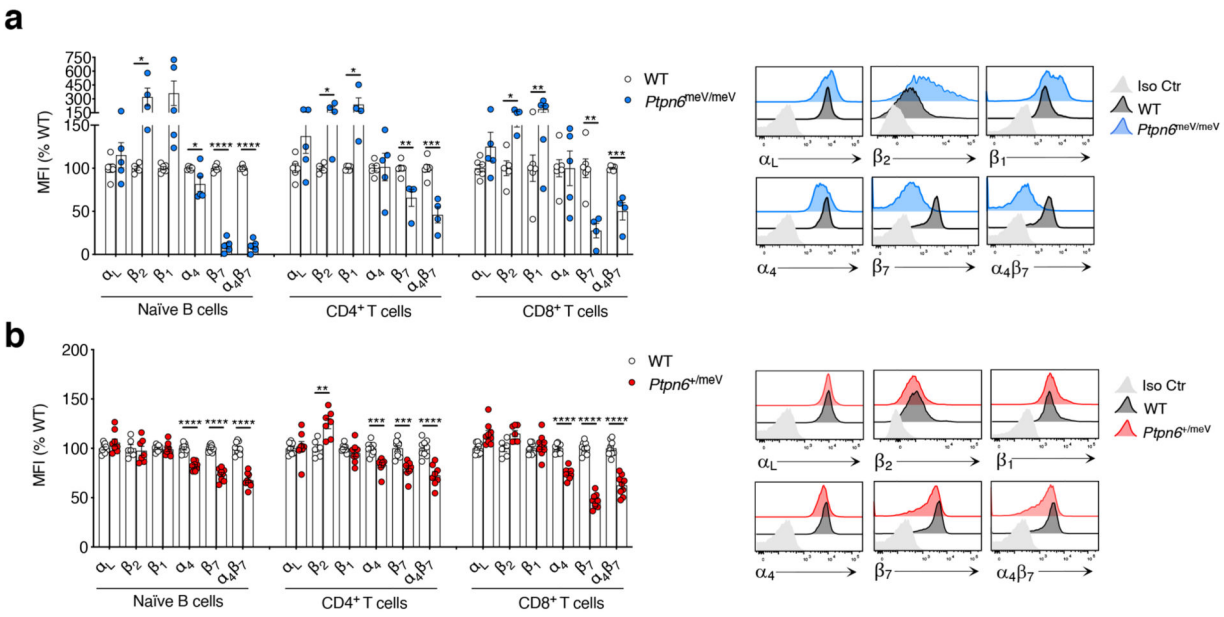

Figure 1. Selective reduction of integrin $\alpha_4\beta_7$ on *motheathen viable* B and T cells.

a, Flow cytometry of WT or *motheathen viable* (*Ptpn6* $^{meV/meV}$) splenic naïve B cells (left panel), CD4$^+$ T cells (mid-panel), and CD8$^+$ T cells (right panel) stained for α_L, β_2, β_1, α_4, β_7, or $\alpha_4\beta_7$. Shown are pooled data (mean ± SEM) from n=4 experiments with 1-2 animals per group per experiment (i.e. 4-6 animals per group total). For each animal within one experiment, the MFI of the integrin staining was expressed as a percentage of the mean MFI of the WT group. Representative histogram overlays gated in naïve B cells are shown (Iso Ctr: Isotype control). **b**, Flow cytometry of WT or *Ptpn6* $^{+/meV}$ splenic naïve B cells (left panel), CD4$^+$ T cells (mid-panel), and CD8$^+$ T cells (right panel) stained for α_L, β_2, β_1, α_4, β_7, or $\alpha_4\beta_7$. Shown are pooled data (mean ± SEM) from n=4 experiments with 4-9 animals per group total. Groups were compared using two-tailed Student's t-test. *P ≤ 0.05, **P ≤ 0.01, ***P ≤ 0.001 and ****P≤0.0001.

Europe PMC Funders Author Manuscripts
Europe PMC Funders Author Manuscripts

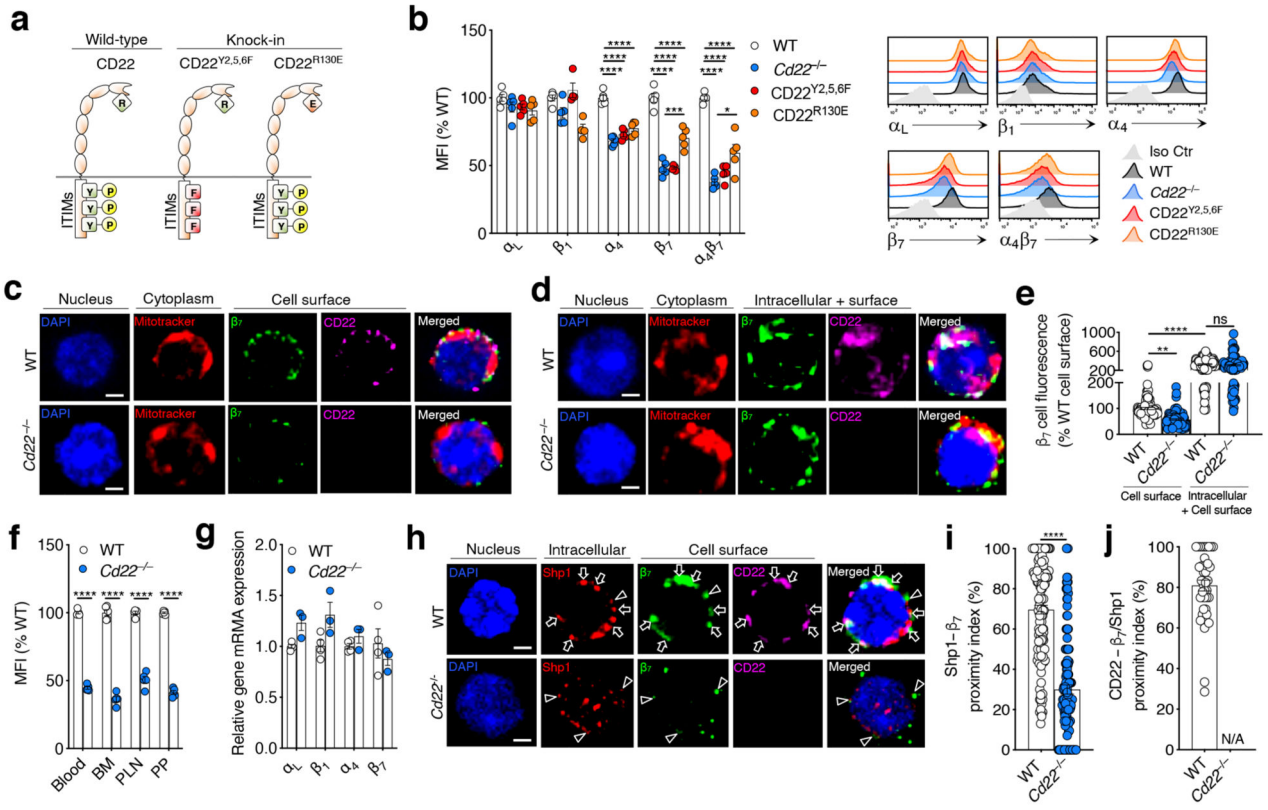

Figure 2. CD22 mediates the Shp1-dependent $\alpha_4\beta_7$ augmentation in B cells.

a, Scheme of wild-type CD22, $CD22^{Y2,5,6F}$, and $CD22^{R130E}$ mutants. **b**, Flow cytometry of WT and CD22 mutant splenic B cells stained for α_L, β_1, α_4, β_7, or $\alpha_4\beta_7$. Shown are pooled data (mean ± SEM) from n=3 experiments with 7 animals per group total analyzed and presented as in Fig. 1. Representative histogram overlays gated in naïve B cells are shown (Iso Ctr: Isotype control). **c-d**, Immunofluorescent staining of cell surface (c) and intracellular (d) β_7 and CD22 in B cells with nucleus (DAPI, blue); cytoplasm (MitoTracker™ Deep Red, Red); β_7 (green) and CD22 (magenta). Scale bars: 2 μM. **e**, For each cell as shown in (c,d), we quantified the intensity of the β_7 fluorescence. Shown are pooled data (mean ± SEM) from three independent experiments with ~100 cells total analyzed per condition. The mean of the β_7 fluorescence intensity for the WT Cell Surface group was set to 100, and data shown as a percentage of this total. **f**, Flow cytometry of WT or *Cd22*$^{-/-}$ B cells isolated from blood, bone marrow (BM), peripheral lymph nodes (PLN), and Peyer's patches (PP) and stained for $\alpha_4\beta_7$ or isotype-matched control. Shown are pooled data (mean ± SEM) from n=2 independent experiments with five animal per group total. **g**, mRNA expression of α_L, β_1, α_4, and β_7 integrins in B cells from WT and *Cd22*$^{-/-}$ mice. Shown are pooled data (mean ± SEM) from two independent experiments with three to four animals per group. **h**, Immunofluorescent staining of intracellular Shp1 and cell surface β_7 and CD22 in B cells with nucleus (DAPI, blue); Shp1 (red); β_7 (green); and CD22 (magenta). Arrow heads: Shp1– β_7 colocalization. Arrows: CD22–Shp1–β_7 colocalization. **i,j**, For each cell as shown in (h), we calculated Shp1–β_7 (i) and CD22 – Shp1/ β_7 (j)

Europe PMC Funders Author Manuscripts
Europe PMC Funders Author Manuscripts

proximity indexes (see Methods). Shown are pooled data (mean ± SEM) from two independent experiments with 130 cells total (i) and 40 cells total (j) analyzed per condition. Groups were compared using One-way ANOVA with Dunnett's multiple comparison test (b,e), and two-tailed Student's t-test (f,g,i). N/A: not applicable. *P ≤ 0.05, **P ≤ 0.01, ***P ≤ 0.001 and ****P≤0.0001.

Europe PMC Funders Author Manuscripts

Europe PMC Funders Author Manuscripts

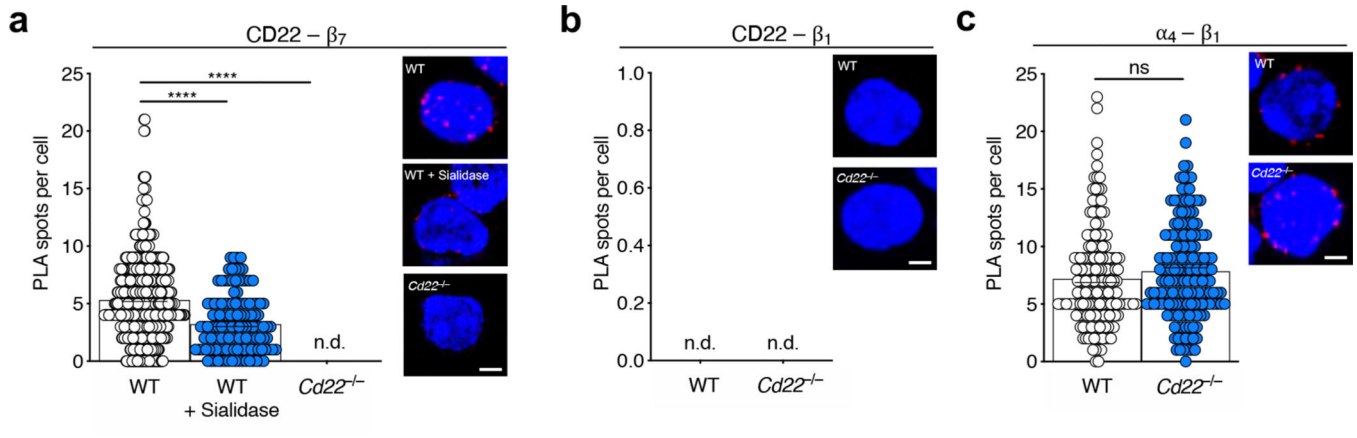

Figure 3. Direct physical association of CD22 and β_7.

a, Association between CD22 and integrin β_7 was assessed by proximity ligation assay (PLA) using purified B cells from wild-type either untreated (WT) or sialidase-treated (WT+ Sialidase), or *Cd22*$^{-/-}$ animals. **b**, Association between CD22 and integrin β_7 was assessed as a negative integrin control. **c**, Association between α_4 and β_1 were analyzed as a positive control for the β_1 integrin. Shown are pooled data (mean ± SEM) from two independent experiments with ~400 cells analyzed per condition. Scale bars: 2 μM. Groups were compared using One-way ANOVA with Dunnett's multiple comparison test (a) and two-tailed Student's t-test (c). ****P≤0.0001. ns: not significant. n.d.: non detectable.

Europe PMC Funders Author Manuscripts
Europe PMC Funders Author Manuscripts

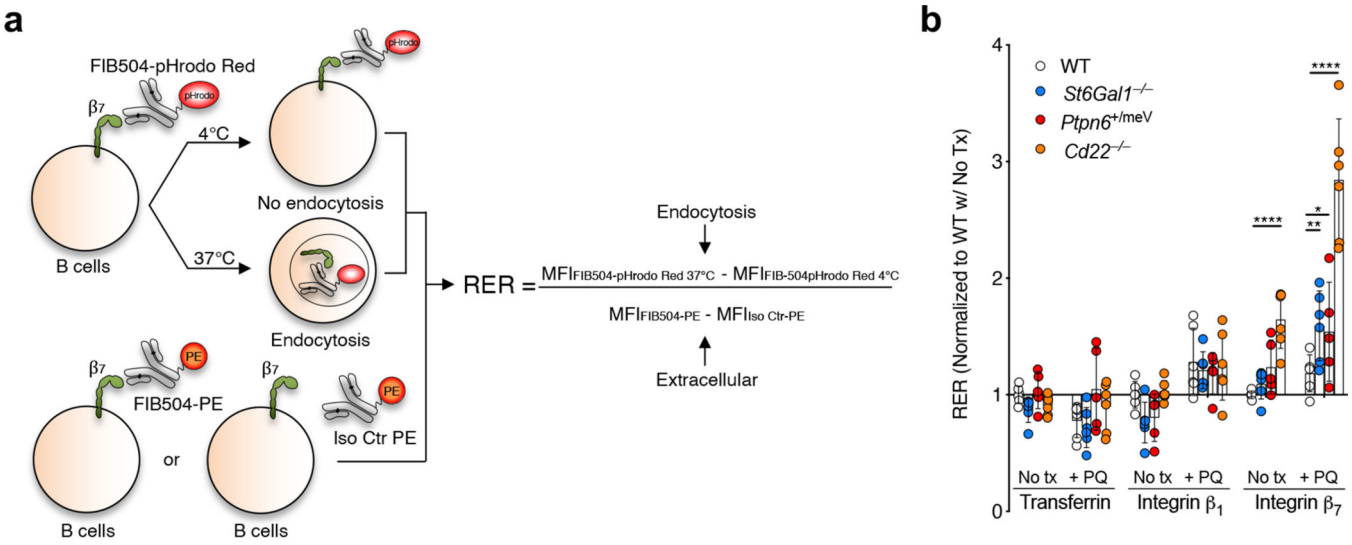

Figure 4. CD22 limits integrin β7 endocytosis in B cells via Shp1 and ligand-recognition.

a, Splenocyte staining with anti-CD19 and anti-IgD (to identify B cells) and pHrodo-Red-conjugated tranferrin (Tf), HMβ1-1 (anti-β_7), or FIB504 (anti-β_7) antibodies at either 4°C (no endocytosis) or 37°C (endocytosis) was used to calculate endocytosis levels (i.e. MFI pHrodo-Red staining at 37°C – MFI pHrodo-Red staining at 4°C). Staining at 4°C with Phycoerythrin (PE)-conjugated RI7217 (anti-Transferrin Receptor 1, TfR1), HMβ1-1, FIB504 or the matching PE-conjugated isotype control antibodies was used to calculate extra-cellular TfR1, β_1, and β_7 levels (i.e. MFI PE staining at 4°C – MFI Isotype Control staining at 4°C). For each molecule (illustrated with β_7 in panel (a)) and each experiment, the Relative Endocytosis Ratio (RER) was calculated by normalizing endocytosis levels to extra-cellular levels. **b**, RER of Tf, β_1, and β_7 in WT, *St6Gal1* $^{-/-}$, *Ptpn6* $^{+/meV}$, and *Cd22* $^{-/-}$ B cells with (100μM) or without primaquine (PQ) treatment. The mean RER of the WT B cells group without PQ (No Tx) was set to 1, and all data were normalized to that mean value. Shown are pooled data (mean ± SEM) from n=3 independent experiments with 6 animals per group total. Groups were compared using Two-way ANOVA with Sidak's multiple comparison test. *P ≤ 0.05, **P ≤ 0.01, and ****P≤0.0001.

Europe PMC Funders Author Manuscripts
Europe PMC Funders Author Manuscripts

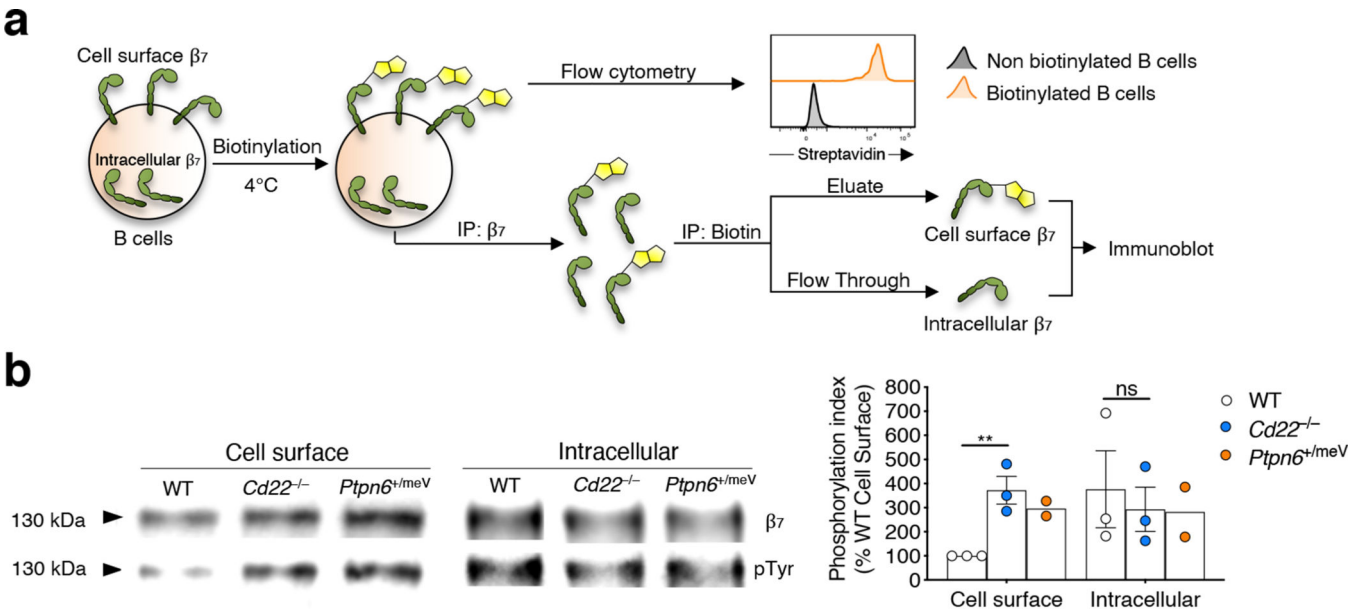

Figure 5. CD22 restrains tyrosine phosphorylation of cell surface β7 integrin in B cells.

a, Scheme of the double immunoprecipitation experiment. Cell surface proteins of purified naïve B cells were biotinylated with Sulfo-NHS-biotin at 4˚C for 1hr. Biotinylation was confirmed by flow cytometry using a streptavidin (SA)-conjugated probe. Biotinylated B cells lysate was used for immunoprecipitation (IP) of β_7 integrin (including biotinylated cell surface β_7 and biotin-free intracellular β_7). Following elution for β_7, a second IP with SA beads was used to recover cell surface β_7 (eluate of the SA-IP) from intracellular β_7 (flow-through of the SA-IP) prior to immunoblot studies. **b**, Left panel: detection of β_7 and phosphotyrosine (pTyr) levels in the cell surface and intracellular β_7 fractions (130 kDa) of wild-type (WT), CD22-deficient (*Cd22* $^{-/-}$), and *Ptpn6* $^{+/meV}$ B cells after the double IP as shown in panel (a). Right panel: quantification of pTyr levels normalized to β_7 levels (pTyr/β_7 ratio). Within each experiment, the pTyr/β_7 of the cell surface β_7 of the WT group was set to 100, and data expressed as a percentage of this total. Shown are pooled data (mean ± SEM) from n=2-3 independent experiments. Each dot represents one independent experiment with n=8 pooled animals for WT and *Cd22* $^{-/-}$ (i.e. n=24 animals total for n=3 independent experimental replicates) and n=4 pooled animals for *Ptpn6* $^{+/meV}$ (i.e. n=8 animals total for n=2 experimental replicates). Data were analyzed using two-tailed Student's t-test. **P ≤ 0.01. ns: not significant.

Europe PMC Funders Author Manuscripts
Europe PMC Funders Author Manuscripts

Europe PMC Funders Author Manuscripts

Europe PMC Funders Author Manuscripts

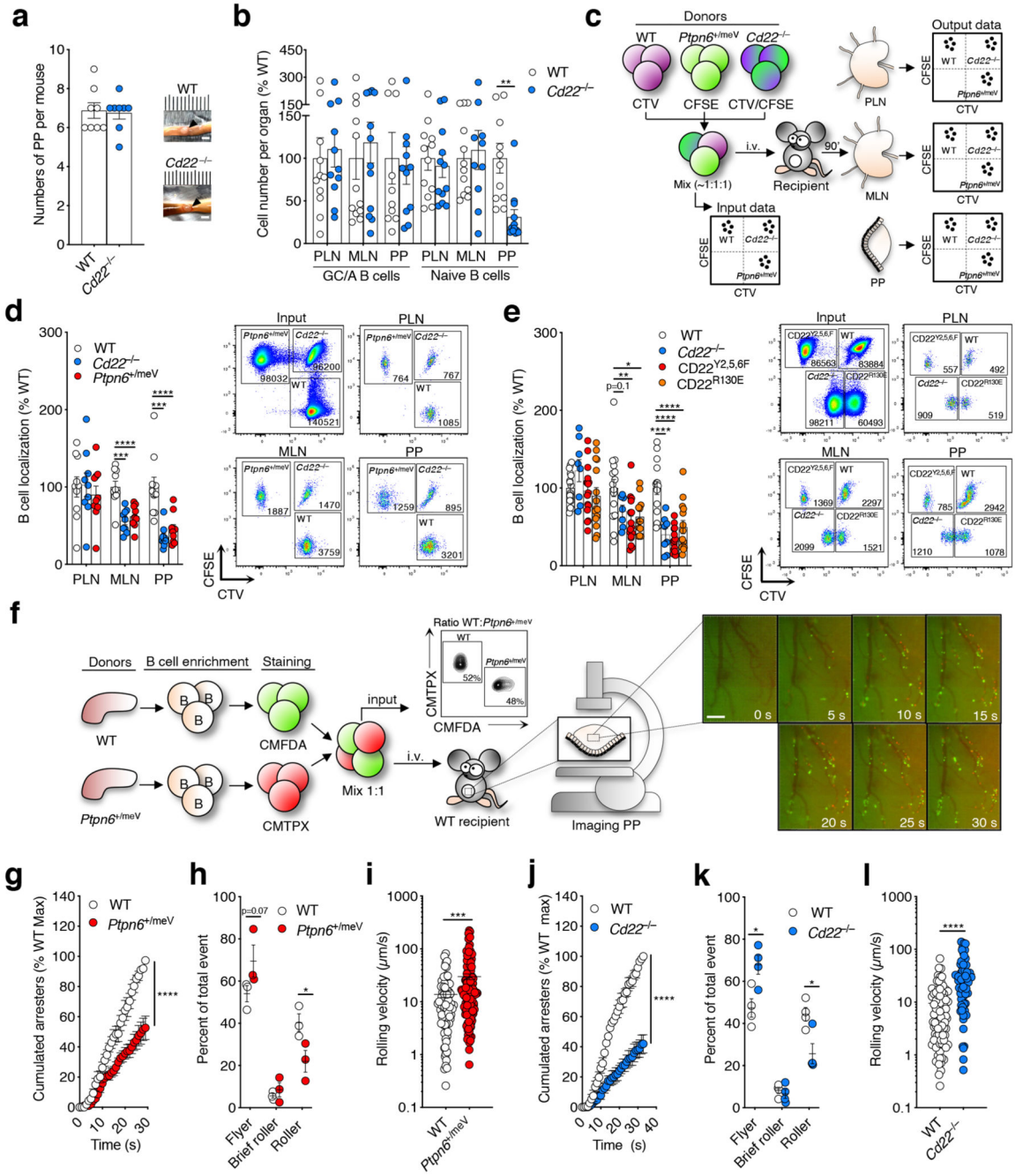

Figure 6. Functional assays reveal defective PP homing and altered endothelial interactions of *Ptpn6* $^{+/meV}$ B cells and *Cd22* $^{-/-}$ B cells

a, Numbers of PP in WT and *Cd22* $^{-/-}$ B cells. Representative PP images from WT and *Cd22* $^{-/-}$ indicated with arrowhead. Scale bars: 2 mm **b**, Numbers of germinal center/ activated B cells (GC/A, CD19^{+} IgD^{-}) and naïve B cells (CD19^{+} IgD^{+}) in MLN, PLN, and PP of WT and *Cd22* $^{-/-}$ shown as a percentage of the mean of the WT group. Shown are pooled data (mean ± SEM) of n=2 experiments with 11-12 mice per group total. **c**, Scheme of short-term homing assay. **d,e**, Localization of WT, *Cd22* $^{-/-}$ and *Ptpn6* $^{+/meV}$ B cells (d) or

Europe PMC Funders Author Manuscripts

Europe PMC Funders Author Manuscripts

WT, *Cd22*$^{-/-}$, CD22^{Y2,5,6F}, and CD22^{R130E} B cells (e) in PLN, MLN and PP after homing assays. Data are shown as a percentage of the mean localization ratio of the WT group. Shown are pooled data (mean ± SEM) of n=3-5 experiments with 11-16 mice per group total. Representative dot plots gated on naive B cells are shown. **f**, Scheme of *in situ* video microscopy experiment. Representative movie pictures are shown with WT B cells (green) and *Ptpn6*$^{+/meV}$ (red). Scale bar: 100 mm. **g-l**, Data in panels (g,h,j,k) represent the mean ± SEM of three independent experiments. **(g,j)** Number of WT vs. *Ptpn6*$^{+/meV}$ (g) or WT vs. *Cd22*$^{-/-}$ (j) arresters on PP HEVs shown second per second from the first cell entering the HEVs. The total amount of WT B cells arresters at the end each experiment (i.e. WT B cells max; ~ 40–80 cells in average) was set to 100, and the data expressed as a percentage of this total. **h,k**, The behavior (i.e. flyer, brief roller, or roller as defined in Extended Data Fig. 7) of each cell entering the HEVs was analyzed in 3-4 representative PP-HEVs per experiment. Results are shown as a percentage of the total numbers of cells entering HEVs (~ 250–300 cells analyzed per group) **(i,l)** Average rolling velocity (mean ± SEM) of representative rollers from n=3 experiments. Groups were compared using two-tailed Student's t-test (a,b,h,i,k,l), paired two-tailed Student's t-test (g,j), and One-way ANOVA with Dunnett's multiple comparison test (d,e). *P ≤ 0.05, **P ≤ 0.01, ***P ≤ 0.001 and ****P≤0.0001.

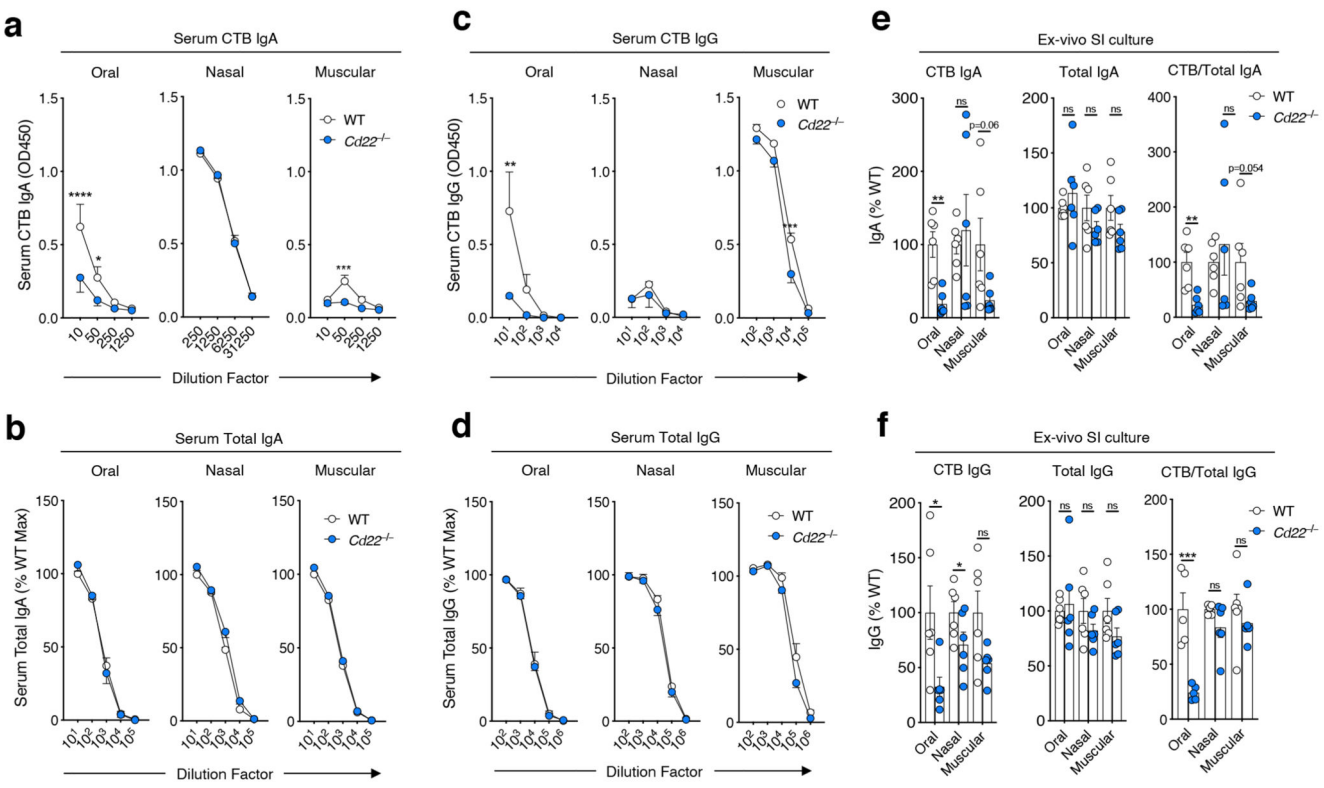

Figure 7. Defects in intestinal responses to oral antigen in CD22-deficient mice.

Cohorts of WT or *Cd22* $^{-/-}$ mice were immunized with Cholera Toxin B (CTB) via the Oral, intra-nasal (Nasal), or intra-muscular (Muscular) routes for two weeks. **a-d**, The serum levels of CTB-specific IgA (a), total IgA (b), CTB-specific IgG (c), total IgG (d) were measured by ELISA and expressed as net OD450 or percentage of the mean OD450 measured in the lowest dilution factor of the WT group. **e,f**, SI segments were cultured *ex vivo* for three days to titer the quantity of secreted CTB-specific IgA, total IgA, and CTB-specific IgA normalized to total IgA (e) and CTB-specific IgG, total IgG, and CTB-specific IgG normalized to total IgG (f) produced by ELISA and expressed as a percentage of the WT group mean. Shown are pooled data (mean ± SEM) from n=2 experiments with 5-6 mice per group total. Groups were compared using Two-way ANOVA with Sidak's multiple comparison test (a-d), and two-tailed Student's t-test (e,f). *P ≤ 0.05, **P ≤ 0.01, ***P ≤ 0.001 and ****P≤0.0001. ns: not significant.

Europe PMC Funders Author Manuscripts
Europe PMC Funders Author Manuscripts

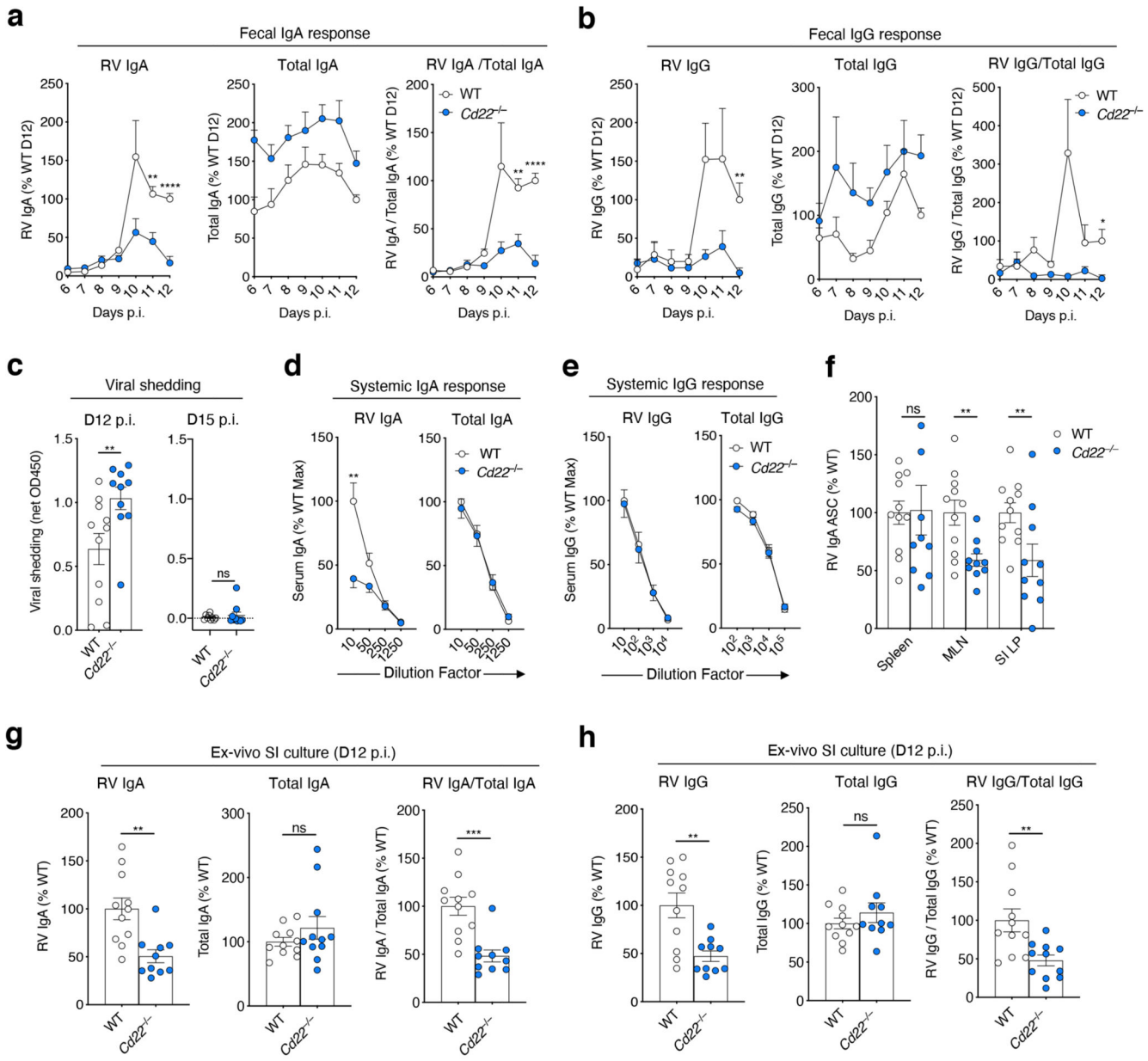

Figure 8. Delayed protective immune response to RV infection in CD22-deficient animals.

a-c, Five days old WT or *Cd22* $^{-/-}$ pups were orally gavaged with the RV strain EW. The production of RV-specific IgA, total IgA, and RV IgA normalized to total IgA (a) or RV-specific IgG, total IgG, and RV IgG normalized to total IgG (b) in fecal samples was measured by ELISA up to twelve days post-infection (D12 p.i.). The mean of the OD450 for the WT group at D12 p.i. was set to 100, and data expressed as a percentage of this total. **c**, Fecal RV Ag shedding as measured by ELISA and expressed as net OD450, normalized to the sample weight. Shown are pooled data (mean ± SEM) from n=4 independent experiments with 10-15 animals per group total. **(d-h)** In separate experiments, five days old WT and *Cd22* $^{-/-}$ pups were orally inoculated with RV EW and sacrificed at day 12 p.i. **d,e**, The serum levels of RV-specific IgA and total IgA (d) and RV-specific IgG and total IgG (e)

Europe PMC Funders Author Manuscripts
Europe PMC Funders Author Manuscripts

Europe PMC Funders Author Manuscripts

Europe PMC Funders Author Manuscripts

were measured by ELISA. The mean of the maximal OD450 for the WT group was set to 100, and data expressed as a percentage of this total. **(f)** The numbers of RV-specific IgA antibody secreting B cells (ASC) were measured in the spleen, MLN, and SI lamina propria (SI LP) by ELISPOT. Shown are numbers of RV IgA ASC per 10^6 total cells expressed as a percentage of the WT group mean. **g,h**, SI fragment cultures. Data are displayed and presented as in Fig. 7e,f to show RV IgA, total IgA, ratios of RV IgA/total IgA (g) and RV IgG, total IgG, ratios of RV IgG/total IgG (h) measured by ELISA. Shown are pooled data (mean ± SEM) from n=2 experiments with 10-11 mice per group total. Groups were compared using Two-way ANOVA with Sidak's multiple comparison test (a,b,d,e), and unpaired two-tailed Student's t-test (c,f,g,h). *P ≤ 0.05, **P ≤ 0.01, ***P ≤ 0.001 and ****P≤0.0001. ns: not significant.